ANNALS OF MICROSCOPY

Vol 13, April 2013

Published under the auspices of
Microscopy Society (Singapore)

SCOPE OF THE JOURNAL

The "Annals of Microscopy" provides an international forum for researchers in biological, physical and materials sciences to present and discuss new research on microscopy.

Fields of interest include: all forms of microscopy. Image acquisition and improvement techniques, along with computer-aided microscopy and analysis are included.

The journal publishes short communications, technical or scientific articles and reviews. Regular articles feature reports of new instrumentation, new theoretical methods and their applications to microstructural analysis in a broad range of fields in biological, physical and material sciences.

The journal also publishes selected news and commentaries of interest to members of microscopy societies and others working in the field of microscopy and microanalysis.

EDITORIAL BOARD

ISSN: 0219-2209

Contents

Harmful Algal Species in the Tebrau Strait: An SEM Observation of the Dinoflagellate Assemblage

Toh-Hii Tan[1], Po Teen Lim[2], Mohd Razali, Roziawati[3] and Chui-Pin Leaw[1]*

[1] Institute of Biodiversity and Environmental Conservation, Universiti Malaysia Sarawak, 94300 Kota Samarahan, Sarawak, Malaysia

[2] Faculty of Resource Science and Technology, Universiti Malaysia Sarawak, 94300 Kota Samarahan, Sarawak, Malaysia

[3] Fisheries Research Institute Batu Maung, Department of Fisheries Malaysia, 11960 Batu Maung, Pulau Pinang, Malaysia

**** Corresponding author:***

Institute of Biodiversity and Environmental Conservation, Universiti Malaysia Sarawak, 94300 Kota Samarahan, Sarawak, Malaysia

Email: cpleaw@ibec.unimas.my, chuipinleaw@gmail.com Tel: +6082 583005 Fax: +6082 583004

ABSTRACT

Harmful algal bloom (HAB) is a natural phenomenon due to the increase of algal cell density in the water column that subsequently causes deleterious effects to natural environments as well as mankind. HABs in the country mainly occurred when a particular group of dinoflagellate cells proliferate in the eutrophied semi-enclosed coastal water body. In this study, dinoflagellate species composition in the Tebrau Strait was determined by scanning electron microscope (SEM). Plankton samples were collected by a 20-micron plankton net haul at several locations of the strait. Samples were undergone fixation, serial dehydration and followed by critical point drying. Samples were then observed under a JEOL analytical SEM. Total of 11 dinoflagellate species were identified, with 7 species known to be associated with HABs events. The occurrence of a fish-killing unarmoured dinoflagellate, *Karlodinium veneficum* was reported for the first time from Malaysian waters. The presence of this and other potentially harmful dinoflagellate species in the strait should be taken seriously by the respective authorities in future expansion of aquaculture industry in the strait.

Keywords: Dinoflagellates, Tebrau Strait, SEM, morphology, *Karlodinium veneficum*.

INTRODUCTION

Malaysia is a country surrounded by waters with a total coastline of 4,675 km, and Johore is one of the states in the Peninsula that has the longest coastline. Aquaculture industry in the state is rapidly growing particularly in the Strait of Tebrau. Other than cockles and shrimp farming, culture of marine fishes in floating cages is one of the common aquaculture activities in the strait.

Harmful algal blooms (HABs) are not uncommon to the country, with increasing frequency and distribution over the last decade. New records of HAB species and expansion of places affected with these events have been reported (Lim *et al*., 2004; Usup *et al*., 2002). Parallel elevation of both aquaculture activities and HAB events in the country has triggered the issues of seafood safety as well as environmental deteriorations due to aquacultural activities. The current knowledge on the occurrence of HAB species in the country particularly in the Strait of Tebrau is far lacking. The only reported HAB outbreak in the strait was the blooms of *Prorocentrum minimum* in 2002 (Usup *et al*., 2004). This information will be of crucial importance for future assessment and mitigation purposes.

In the present study, we aim to document the dinoflagellate assemblages as a species inventory in the Straits of Tebrau, particularly of those that are harmful. Plankton samples were collected from two selected sites and the dinoflagellate species were examined by using scanning electron microscope (SEM). This study was carried out at locations with intensive aquaculture activities on-going. By using this species inventory of harmful dinoflagellates we hope to provide further information to respective country authorities in monitoring and mitigating HABs as well as selection of aquaculture sites.

MATERIALS AND METHODS

Samples were collected using a 20-µm plankton net from the waters in the Tebrau Strait between July and December, 2009 (Fig. 1). Samples collected through net hauls were preserved in Lugol's solution in the field. Samples brought back to the laboratory were kept at 4ºC in the dark for further analysis. Samples were prepared for SEM observation as described in Leaw *et al*. (2010). In brief, preserved samples were fixed in 5% glutaraldehyde. The fixed samples were filtered on a 0.2 µm black polycarbonate membrane filter, and rinsed a few times with cacodylate buffer (0.1 M, pH 7) through a vacuum manifold. Samples were then enclosed in a filter paper envelope and dehydrated with a graded series of ethyl alcohol concentration (30%, 50%, 70%, 80%, 90%, 95%, and 100%) for 15 min each, and twice in the intermedium, amyl acetate for 15 min each. Samples were then undergone critical point drying (CPD). Dried samples were mounted on to a stub, and coated with gold-palladium using a JEOL JFC-1600 magnetron sputter coating instrument (JEOL, Japan). Samples were then viewed under a JEOL JSM-6510 analytical scanning electron microscope (JEOL, Japan).

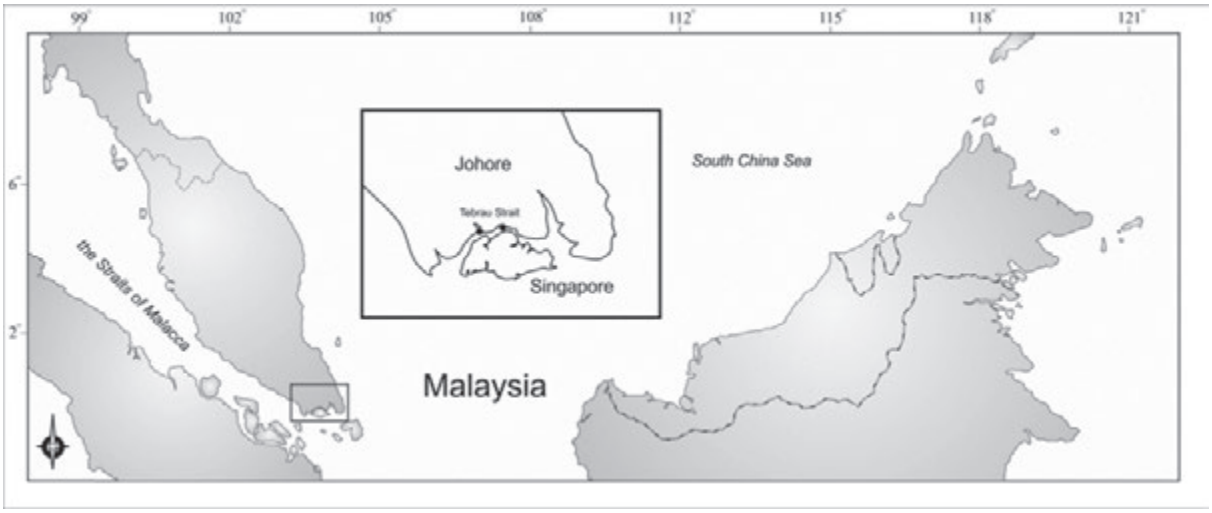

Fig. 1 Map of Tebrau Strait showing two sampling locations in this study.

RESULTS & DISCUSSION

A total of 11 species of dinoflagellates were identified in this study. Phytoplankton bloom was observed in the field samples collected during July and December 2009. Among the species identified, 7 were harmful either as fish killers or toxin producers (Table 1) which encountered more than half of the species found (60%). Morphology of each species found in the strait is described herewith based on the SEM observation of the outer cell structures. It is notable that a fish-killing unarmoured dinoflagellate, *Karlodinium veneficum* is found for the first time in Malaysian waters. This record of occurrence is a first record ever in Malaysia.

Species description

***Karlodinium veneficum* (D. Ballantine) J. Larsen 2000**

Synonyms

The first name ever given to this species (basionym) was *Gymnodinium veneficum* (Ballantine, 1956). This athecate species was also known as *Karlodinium micrum* (Leadbeater et Dodge) Larsen (Daugbjerg *et al.*, 2000), *Gymnodinium galatheanum* (Braarud sensu Kite et Dodge), *Gymnodinium micrum* (Leadbeater et Dodge) Loeblich III, *Gyrodinium galatheanum* (Braarud) Taylor and *Woloszynskia micra* (Leadbeater et Dodge) (Bergholtz *et al.*, 2006).

Table 1 Harmful species of dinoflagellates found in the Tebrau Strait.

Species	Impact
Dinophysis acuminata	Diarrhetic shellfish poisoning (DSP)-toxins producer
Dinophysis caudata	DSP-toxins producer
Karenia mikimotoi	Fish killer
Karlodinium veneficum	Fish killer (ichthyotoxin, karlotoxin producer)
Neoceratium furca	Fish killer
Prorocentrum micans	Bloom forming species, shellfish killer
Scrippsiella trochoidea	Non toxic fish killer

Diagnosis

Cells are small and ovoid without dorso-ventral compression (Fig. 2). Cells are with length of 18 – 22 µm and width of 14 – 18 µm (n = 4). Cells are slightly bigger than those reported which ranged in 9 – 18 µm in length and 7 – 14 µm in width (Ballantine, 1956; Dodge, 1982; Taylor *et al.*, 1995).

The epicone and hypocone are equal in size (Fig. 2A, B). The cell's anterior end is slightly pointed. Ventral pore is situated on the left side of the apical groove. The ventral pore is not rounded but slightly elongated ventrally (Fig. 2A). Apical groove present at the epitcone starting from the apical-ventral of the cell towards the dorsal side (Fig. 2C).

Hypocone is rounded with a slight indentation at its posterior end. The deep cingulum is displaced in a descending spiral of 3 times its width. The sigmoid-shaped sulcus slightly invades the epicone (Fig. 2B). The sulcus is deeply excavated and displaced 3 times into the hypocone on the right ventral side (girdle width = 2.0 µm, girdle displacement = 5.03 µm, n = 4) (Fig. 2B).

Generally, the features are similar to the description of *K. veneficum* by Ballantine (1956), Dodge (1982), and Taylor *et al*. (1995). Cell dimensions are in the range of *K. armiger* Bergholtz, Daugbjerg & Moestrup, *K. australe* de Salas, Bolch & Hallegraeff, *K. conicum* de Salas, but dissimilar from other *Karlodinium* species described (Table 2). It differs from *K. armiger* by the cingulum displacement where *K. armiger* is with two cingulum widths and approximately one-third of the cell length. Whereby the cells observed in this study have 3 times cingulum width, displaced roughly 20% of the cell length. The cells differ from *K. australe* and *K. decipiens* by the deeply excavated cingulum, where both latter species possess shallow cingulum. No longitudinal furrow is observed in the cells which is the distinctive feature of *K. corrugatum* de Salas.

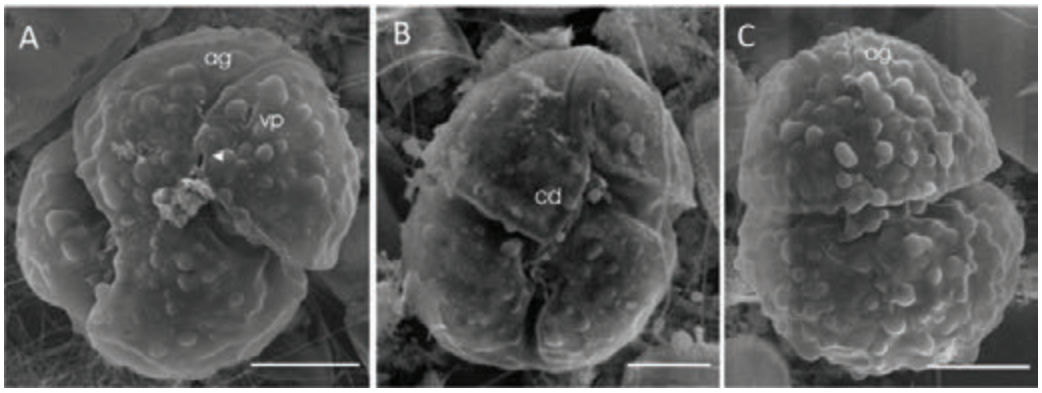

Fig. 2 Scanning electron micrographs of *Karlodinium veneficum* from the Tebrau Strait, Johor. (A) Apical-dorsal view showing elongated ventral pore (vp) and apical groove (ag). (B) Dorsal view of cell showing the cingulum displacement (cd) descending to the right. (C) Ventral view of cell showing the starting of apical groove. Scale bar = 5 µm.

Toxicity/harmful effect

The species was reported to produce karlotoxin, an ichthyiotoxin (Peng *et al.*, 2010), that are lethal to fish through damage of gill epithelia (Deeds *et al*., 2006; Hernández-Becerril *et al*., 2000). A study by Kempton *et al*. (2002) reported that blooms of *K. veneficum* had caused fish kills in the hybrid striped bass aquaculture pond in Chesapeake Bay (Kempton *et al*., 2002).

***Dinophysis acuminata* Claparède and Lachmann, 1859**

Cell is oval or elliptical shape and rounded from the posterior. Cell has a high cingulum with list giving a small cap-like epitheca and a large hypotheca. The theca surface is covered with pores. The sulcus list extends to half the body length. There are lesser and smaller pores at the megacytic zone that looks smoother compared to the pores in the middle of the hypotheca (Fig. 3A). The left sulcal list is well developed and extends beyond the midpoint of the cell and is of equal depth.

Toxicity/ harmful effect

This species has been reported to produce okadaic acid (Cembella & Therriault, 1989; Lee *et al*., 1989) and associated with DSP cases (Kat, 1985).

***Dinophysis caudata* Saville-Kent, 1881**

The cell is laterally compressed with a small cap-like epitheca and a very large hypotheca (Fig. 3B). Cells are around 81-91 μm in length and 45-65 μm in dorso-ventral width (at base of LSL). The cell's dorsal side curve gradually to the anterior part of the hypotheca. There is a large and long projection at the hypotheca towards the posterior end. The cingulum is narrow with two well-developed lists. The anterior cingular list is wider than the posterior cingular list. Both cingular lists are supported by ribs and form a funnel shape which hides the epitheca. There is a long and big left sulcal list which contains three ribs and its length is almost half the total length. The thecal plate is heavily aerolated and each contains a pore.

Toxicity/ harmful effect

This species had been reported to produce pectenotoxins (Miles *et al*., 2004).

***Diplopsalis lenticula* Bergh, 1881**

The cells are subspherical to lenticular shape (Fig. 3C), with length of 23-48 μm and diameter of 32-68 μm. The epitheca and hypotheca are divided equally by the circular, median cingulum. Cell surface is smooth with scattered pores. Cingular lists are supported by fine ribs which are broad and projecting laterally. The left sulcal list is bigger than the right sulcal list and curved to the right. The species is non-toxic.

***Gyrodinium spirale* (Bergh, 1881) Kofoid et Swezy, 1921**

Cell is large with the length of 100 μm and width of 35.7 μm (Fig. 3D). Cingulum is excavated and narrow. The displacement is more than one-third of the body length (displacement = 42.8 μm). It has a pointed apex curved to the right side. There are body ridges from the apical to antapical. The cell observed is slightly longer compared to the original description with the cell length of 70 – 80 μm and width of 30 μm (Rangel *et al*., 2004). A characteristic feature of this species is the longitudinal surface ridges.

Toxicity/ harmful effect

Gyrodinium spirale was reported to produce PSP toxins and cause fish mortality in Luanda Bay, Angola in September 2002 (Rangel *et al*., 2004).

***Karenia mikimotoi* Miyake et Kominami ex Oda, 1935**

Cell is without thecal plates. Cell is small, broadly oval to almost round, slightly longer

Table 2 Morphological comparison of species in the genus of *Karlodinium*. Morphological characteristics of each species were compiled from literatures (Bergholtz et al., 2006; Daugbjerg, 2000; De Salas et al., 2005; De Salas et al., 2008; Siano et al., 2009).

	Species								
	K. antarcticum	*K. armiger*	*K. australe*	*K. ballantinum*	*K. conicum*	*K. corrugatum*	*K. decipiens*	*K. veneficum*	*K. vitiligo*
Cell shape	Elongated and ovoid	ovoid	ovoid	Small & ellipsoidal	Pentagonal outline	Biconical to pentagonal	ellipsoidal	Broadly elliptical, circular cross-section	Ovoid, small
Length (μm)	15-24	12-22	19-26	11-18	19-29	13-21	18-25	8-18	7-18
Width (μm)	10-14	8-18	16-22	8-14	15-25	11-17	13-19	8-14	7-14
Apical groove	very long, extending through most of the ventral side and halfway down the dorsal side of the epicone	Extends above sulcal extension on ventral side of cell. Slightly curve, bypasses apex. Extends one-forth the length of the epicone on dorsal side	Apical groove short and straight, extending only briefly onto the dorsal side of the epicone	very short and linear, extending less than halfway down the ventral epicone and very briefly down the dorsal side	short, covering 1/3 of the ventral epicone and 1/4 of the dorsal side	medium length, originating above the anterior end of the sulcus and extending 1/4 of the way down the dorsal epicone	linear, originating parallel to the level of the apical margin of the cingulum and extending to halfway down the dorsal epicone	Straight descending one-seventh down the dorsal epicone.	

	Species								
	K. antarcticum	*K. armiger*	*K. australe*	*K. ballantinum*	*K. conicum*	*K. corrugatum*	*K. decipiens*	*K. veneficum*	*K. vitiligo*
Ventral pore	Pore located high on ventral side	Elongate ventral pore on left side of epicone	Left of sulcal extension	Absent or inconspicuous	Large, approx halfway between the anterior sulcal termination and beginning of apical groove	A thin, long slit located well to the left of the sulcal region.			Anterior pore at the junction of the left side of the girdle and slcus, posterior pore at the junction of right side girdle and sulcus.
Cingulum	Shallow and wide	Anterior side delineated sharply from epicone, posterior extending smoothly into hypocone		Deeply excavated		Wide and deeply excavated, with prominent margins	Shallow and wide	Equatorial, deep and narrow	deeply impressed, narrower on the ventral side
displacement	1/3-1/2 of cell length	2 cingulum width, 1/3 of cell length	1/4 of cell length	1/3 of cell length	1/4 of cell length	1/4 of the cell length	1/3 of the cell length	2 girdle widths	two girdle widths

(19.84 μm) than wide (18.31 μm) with a characteristic long and straight apical groove to the right of the sulcal axis (Fig. 3E). Epicone is broadly conical and smaller than the hypocone. Hypocone is notched by the widening sulcus at the antapex resulting in a lobed posterior. The wide and deeply excavated cingulum is pre-median, and is displaced in a descending spiral about 2 times the cingulum width.

Toxicity/ harmful effect

The species was reported to cause massive killing of fish and shellfish. An ichtyotoxic compound was associated with the species (Silke *et al*., 2005).

***Neoceratium furca* (Ehrenberg) Fernando Gómez, David Moreira, Purificación López-García.**

Synonyms

Ceratium furca (Ehrenberg) Claparède et Lachmann, *Ceratophorus* furca (Ehrenberg) Diesing, *Biceratium furca* Vanhőffen, *Peridinium eugrammum* Ehrenberg.

Diagnosis

Cell is large with two unequal parallel hypotheca horns. The right horn is shorter than the left one. Epitheca has an anterior horn that looks like a funnel. Thecal plates are thick and have linear markings (Fig. 3F). Cell is 130 μm in length and 34 μm in width which is in the range of type specimens (length is between 100 – 250 μm and width of 30 – 50 μm) (Steidinger & Tangen, 1997). The cell is similar to the original description of *Ceratium furca* (Claparède & Lachmann, 1859).

Toxicity/ harmful effect

This species had been reported to cause fish and invertebrate kills (Glibert *et al*., 2002).

***Prorocentrum gracile* Schütt, 1895**

Cell is elongated almost 3 times as longer (64 μm) than wide (22 μm). The shape is pyriform with a pointed posterior end. An anterior spine around 8.3 μm is present at the periflagellar area (Fig. 3G).

Identification of *P. gracile* and *P. micans* can be confusing due to the similar trichocyst pore pattern (Steidinger & Tangen, 1997) and the similar arrangement of the apical spine (Toriumi, 1980). *P. gracile* is much longer with length: width ratio of 2 while *P. micans* has a length: width ratio of <2. Another diagnostic character is the stronger and longer apical spine compare to *P. micans* which has broader and shorter apical spine. This species is non-toxic.

***Prorocentrum micans* Ehrenberg, 1834**

Cells are medium-sized of tear-drop to heart shaped when observed from the valve view. The cell is rounded at the anterior end, broadest at the middle and pointed at the posterior end (Fig. 3H). There is a short anterior spine. The surface is rugose with many trichocyst pores. The intercalary band is big and smooth. Cell dimension is 32.7 μm long and 21.36 μm wide, with the length of spine 3.18 μm (Fig. 3H).

The species was distinguished from others in the genus by the broader and shorter anterior spine. The cell is broadest in the middle with the length: width ratio of less than 2.

Toxicity/ harmful effect

This species is a non-toxic but bloom forming species (Pybus, 1990). It may release diatom growth inhibition substance (Uchida, 1977).

***Protoperidinium marukawai* (Abé) Balech, 1974**

Cells are round and compressed apical-antapically (Fig. 3I). Cingulum with strong ribs observed. Sulcus is short, left sulcal list is larger compares to the right sulcal list. Cell surface is smooth and thecal plates are easily distinguished. Cells are 30.85 um in transdiameter ($n = 2$). The species is non-toxic.

***Scrippsiella trochoidea* (Stein) Loeblich III, 1976**

Cell has cone shape epitheca with a short apical convex and rounded hypotheca (Fig. 3J). Cell is small with the length of 22-25 μm and width of 18-21 μm ($n = 2$). Cell surface is smooth.

Toxicity/harmful effect

This species had been associated with fish kills (Lu & Hodgkiss, 2004).

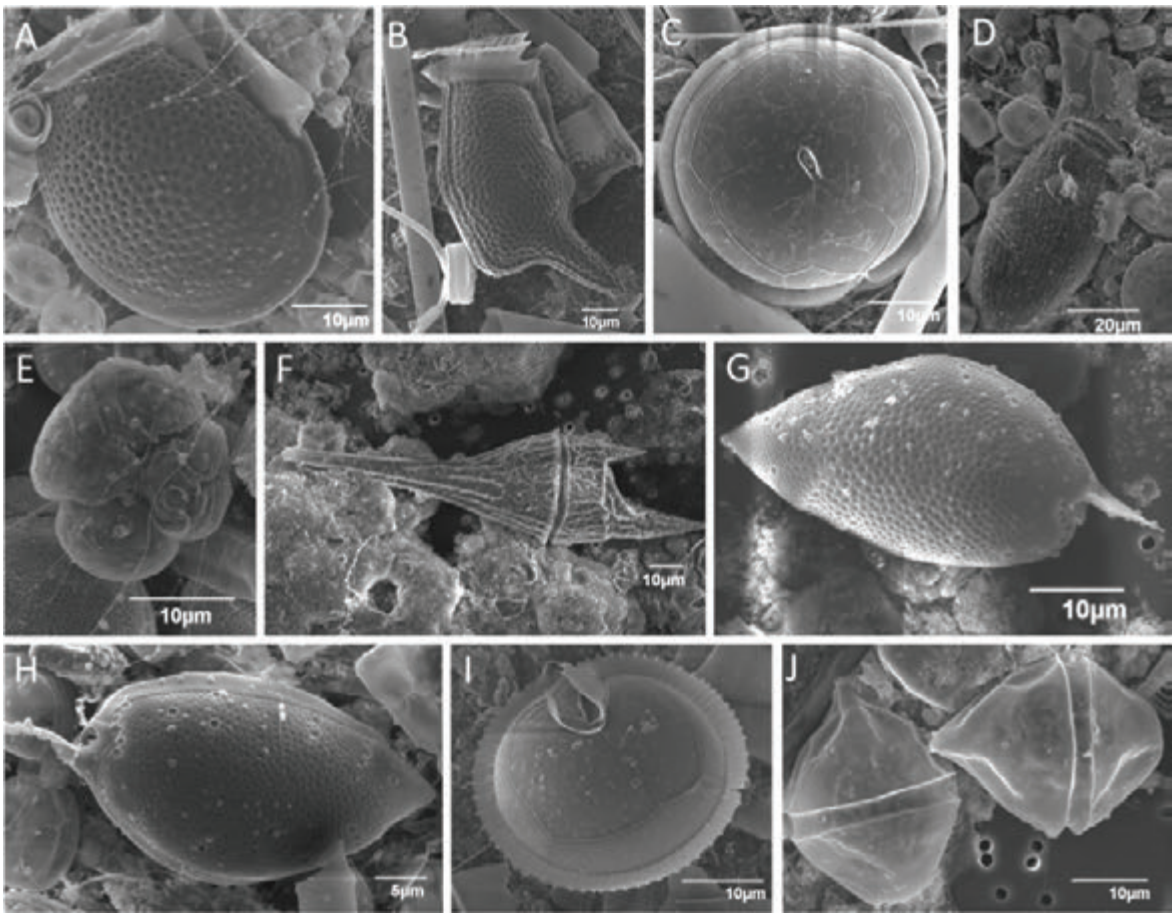

Fig. 3 Scanning electron micrographs of dinoflagellates found in Tebrau Strait, Johore. (A) *Dinophysis acuminata*, (B) *Dinophysis caudata*, (C) *Diplopsalis lenticula*, (D) *Gyrodinium spirale*, (E) *Karenia mikimotoi*, (F) *Neoceratium furca,* (G) *Prorocentrum gracile*, (H) *Prorocentrum micans*, (I) *Protoperidinium marukawai*, (J) *Scrippsiella trochoidea.*

CONCLUSIONS

Among the dinoflagellates observed in the Tebrau Strait, seven are harmful or potentially harmful which were claimed to cause HAB events. However, no incidence of HABs was reported from the area thus far. This study recorded for the first time the occurrence of *Karlodinium micrum*, a fish-killing unarmoured dinoflagellate in Malaysian waters. The occurrence of this icthyotoxin producer might affect the mariculture industry in the strait. The presence of this and others potentially harmful dinoflagellate species in the strait should be taken into consideration by the related authorities in future expansion of aquaculture industry in the strait.

ACKNOWLEDGEMENTS

This study was supported by the Malaysian Government through ScienceFund and FRGS to CP Leaw and PT Lim.

REFERENCES

Ballantine, D. 1956. Two new marine species of Gymnodinium isolated from the Plymouth area. *Journal of the Marine Biological Association of the United Kingdom* **35**:467-74.

Bergholtz, T., Daugbjerg, N., Moestrup, O. & Fernández-Tejedor, M. 2006. On the identity of Karlodinium veneficum and description of *Karlodinium armiger* sp. nov. (Dinophyceae), based on light and electron microscopy, nuclear encoded LSU rDNA and pigment composition. *J. Phycol.* **42**:170-93.

Cembella, A. D. & Therriault, J. C. 1989. Population dynamics and toxin composition of *Protogonyaulax tamarensis* from the St. Lawrence estuary. *In*: Okaichi, T., Anderson, D. M. & Nemoto, T. [Eds.] *Red Tides-Biology, environmental Science and Toxicology.* Elsevier, New York, pp. 81-85.

Claparède, É. & Lachmann, J. 1859. Études sur les infusoires et les rhizopodes. *Mémoires de l'Institut National Genevois* **6**:261-482.

Daugbjerg, N., Hansen, G., Larsen, J. & Moestrup, Ø. 2000. Phylogeny of some of the major genera of dinoflagellates based on ultrastructure and partial LSU rDNA sequence data, including the erection of three new genera of unarmoured dinoflagellates. *Phycologia* **39**:302-17.

Deeds, J. R., Reimschuessel, R. & Place, A. R. 2006. Histopathological Effects in Fish Exposed to the Toxins from *Karlodinium micrum*. *Journal Aquatic Animal Health* **18**:136–48.

Dodge, J. D. 1982. Marine Dinoflagellates of the British Isles. *Her Majesty's Stationary Office, London*.

Glibert, P. M., Landsberg, J. H., Evans, J. J., Al-Sarawi, M. A., Faraj, M., Al-Jarallah, M. A., Haywood, A., Ibrahem, S., Klesius, P., Powell, C. & Shoemaker, C. 2002. A fish kill of massive proportion in Kuwait Bay, Arabian Gulf, 2001: the roles of bacterial disease, harmful algae, and eutrophication. *Harmful Algae* **1**:215-31.

Hernández-Becerril, D. U., Cortés Altamirano, R. & Alonso, R. R. 2000. The dinoflagellate genus *Prorocentrum*; along the coasts of the Mexican Pacific. *Hydrobiologia* **418**:111-21.

Kat, M. 1985. *Dinophysis acuminata* blooms, the distinct cause of Dutch mussel poisoning. *In*: Anderson, D. M., White, A. W. & Baden, D. G. [Eds.] *Toxic dinoflagellates.* Elsevier, New York, pp. 73 - 77.

Kempton, J. W., Lewitus, A. J., Deeds, J. R., Law, J. M. & Place, A. R. 2002. Toxicity of *Karlodinium micrum* (Dinophyceae) associated with a fish kill in a South Carolina brackish retention pond. *Harmful Algae* **1**:233-41.

Lee, J.-S., Igarashi, T., Fraga, S., Dahl, E., Hovgaard, P. & Yasumoto, T. 1989. Determination of diarrhetic shellfish toxins in various dinoflagellate species. *Journal of Applied Phycology* **1**:147-51.

Lim, P.-T., Leaw, C.-P. & Usup, G. 2004. First incidence of paralytic shellfish poisoning on the east coast of Peninsular Malaysia. *In*: Phang, S. M., Chong, V. C., Ho, S. S., Mokhtar, N. & Ooi, J. L. S. [Eds.] *Marine Science into the New Millennium: New Perspectives and Challenges.* University of Malaya Maritime Research Centre, Kuala Lumpur, Malaysia, pp. 661-67.

Lu, S. & Hodgkiss, I. J. 2004. Harmful algal bloom causative collected from Hong Kong waters. *Hydrobiologia* **512**:231-38.

Miles, C. O., Wilkins, A. L., Samdal, I. A., Sandvik, M., Petersen, D., Quilliam, M. A., Naustvoll, L. J., Rundberget, T., Torgersen, T., Hovgaard, P., Jensen, D. J. & Cooney, J. M. 2004. A novel pectenotoxin, PTX-12, in *Dinophysis* spp. and shellfish from Norway. *Chemical Research in Toxicology* **17**:1423-33.

Peng, J., Place, A. R., Yoshida, W., Anklin, C. & T.Hamann, M. 2010. Structure and Absolute Configuration of Karlotoxin-2, an Ichthyotoxin from the Marine Dinoflagellate *Karlodinium veneficum*. *Journal of the American Chemical Society* **132**:3277-79.

Pybus, C. 1990. Blooms of Prorocentrum Micans (Dinophyta) in the Galway Bay area. *Journal of the Marine Biological Association of the United Kingdom* **70**:697-705.

Rangel, M., Muai, J. & Silva, S. 2004. Mortality caused by dinoflagellates bloom in Luanda. *Harmful Algae News, The Intergovernmental Oceanographic Commission of UNESCO* **26**:8.

Silke, J., Beirn, F. O. & Cronin, M. 2005. *Karenia mikimotoi*: An exceptional dinoflagellate bloom in western Irish waters, summer 2005. *Marine Environment and Health Series* **21**.

Steidinger, K. A. & Tangen, K. 1997. Dinoflagellate. *In*: Tomas, C. R. [Ed.] *Identifying Marine Diatoms and Dinoflagellates.* Academic Press, New York, pp. 387-598.

Taylor, F. J. R., Fukuyo, Y. & Larsen, J. 1995. Taxonomy of harmful dinoflagellates. *In*: Hallegraeff, G. M., Anderson, D. M. & Cembella, A. D. [Eds.] *Manual on Harmful Marine Microalgae.* IOC Manual and Guides No. 33. UNESCO, Paris, pp. 283-318.

Toriumi, S. 1980. *Prorocentrum* species (Dinophyceae) causing red tide in Japanese coastal waters. *Bulletin of Plankton Society of Japan* **27**:105-12.

Uchida, T. 1977. Excretion of a diatom inhibitory substance by *Prorocentrum micans* Ehrenberg. *Japanese Journal of Ecology* **27**:1 - 4.

Usup, G., Leaw, C. P., Lim, P. T. & Ahmad, A. 2002. Probable toxin producer responsible for the first occurrence of paralytic shellfish poisoning on the east coast of Peninsula Malaysia. *Malaysian Applied Biology* **31**:29-35.

Usup, G., Cheah, M.Y., Rozirwan, Ng, B.K., Leaw, C.P., Othman, M. and Faazaz, A.L. 2004. Identification of the species responsible for the harmful algal bloom event in Selat Tebrau in 2002. *Malaysian Applied Biology* **35**:59-62.

Ultrastructural Description of Young Corn (*Zea mays* L) Ear

Nik Fakurudin N.A., M.A. Solihah and W.I. Wan Rosli*
School of Health Sciences, Health Campus, Universiti Sains Malaysia, 16150 Kubang Kerian, Kelantan, Malaysia.

ABSTRACT

Young corn (*Zea mays* L) ears are small, immature indehiscent fruits that do not open spontaneously at maturity to release seeds. The present ultra structural study was conducted to examine detailed surface structure topography of the young corn ear. Macroscopic observation were done on fresh young corn ears prior to dry-gross sectioning. They were viewed using variable pressure scanning electron microscope (VPSEM). Observation of the longitudinal and horizontal section shows manifestation of anomalous appearances of the pedicel of the cotyledon. The actual area of growth of the corn silk base mimics the structured formation of matured corn fruit were seen in all micrographs. The ultra-structures of the young corn ears consist of the pith cell, pedicel, corn silk roots and pericarp of the cotyledon. Corn silks also present as a single hollow tubular strand with longitudinally-oriented array tubes at every pedicel. The size of these corn silks strands vary between 6-8 μm in diameter. These findings are the first recording describing the VPSEM analysis of the surface ultra structure topography of young corn ears.

Keywords: Young corn ears, Variable Pressure Scanning Electron Microscope (VPSEM)

INTRODUCTION

Young corn (baby corn) is a vegetable obtained from the fruiting corn (*Zea mays*) plant harvested early, while the ear are very small and immature. Young corn consists of the husked ear, harvested two or three days after emergence of the silk (Almeida *et al*. 2005; Lund *et al*. 1958). Many regular corn varieties have been used to grow baby corns. However, the resulting baby corns are often in a relatively poor condition. The stalk grows to about 61 cm high. The baby corn kernel are uniform in shape and petite in size while the ears are typically 4.5 cm to 10 cm in length and 7 mm to 17 mm in diameter (Chutkaew *et al*. 1994). Young corns are most commonly used in Asia. Many varieties of the specialized corn plants were developed to just produce baby corn. This production, being a recent development, has proven to be enormously successful venture and has become one of the most important crop in Thailand and Taiwan (Kasikranan *et al*. 2001).

Baby corns are used as salad, vegetable and cooked as soup and are also pickled. There is no difference in taste between young corns of the sweet corn type and the field corn type (Bar-Zur *et al*. 1993). In the ultra structural study of plant, detailed structure of a various parts of the plant specimen, such as cells, tissues, organs including cellular structures that are too small to be seen with an optical microscope. These structures are then observed under electron microscopy (Amesz *et al.* 2004). To our knowledge, the ultra-structural description of baby corn ears has not been reported to date.

MATERIALS AND METHODS

Sample preparation

Fresh cereal grain of *Zea mays* L (dried cut kernel of *Zea mays* L) were harvested from Bachok, a coastal district area of Kota Bharu, in the state of Kelantan, Malaysia. Ten young corns (approximate 500g) were selected, cleaned and their corn silk removed and gently washed under running tap water. Excessive water was drained off before the samples were subjected to morphological characterization.

Scanning Electron Microscopy

100 grams of the freshly prepared young corn ear samples were either (a) slowly dried in hot air oven with a consistent temperature of 45°C until completely dried (without any treatment) (b) treated by soaking and agitation (Rotamax 120, Heidolph, German) for 24 hours in 4.5% sodium hypochlorite solution. Cross-sections and longitudinal sections of kernels were made and the endosperm cells were studied using Variable Pressure Scanning Electron Microscope (VPSEM). The samples were then slowly dried in a hot air oven with a constant temperature until completely dried. The dried samples were affixed to aluminium specimen stubs using carbon paint. The dried samples were coated with a thin layer of gold in a vacuum evaporator (Baltex SCD005 Sputter Coater, Hi-Tech Germany) and their structure and morphology were studied by a LEO 1455 VPSEM under 5.5 Pascal pressure, using the secondary electron mode, at a working distance of 16-17 mm at 5.0 kV (Wan Rosli *et al*. 2007).

RESULTS AND DISCUSSION

The general morphology of young corn ear shows neatly aligned rows of vestigial grain with ends evenly tapering (fig. 1.). The cross-section of the young corn kernel shows asymmetries of form in a complex manner. The core of the young fruits is round but show variability in relation to its convolutions and pith width.

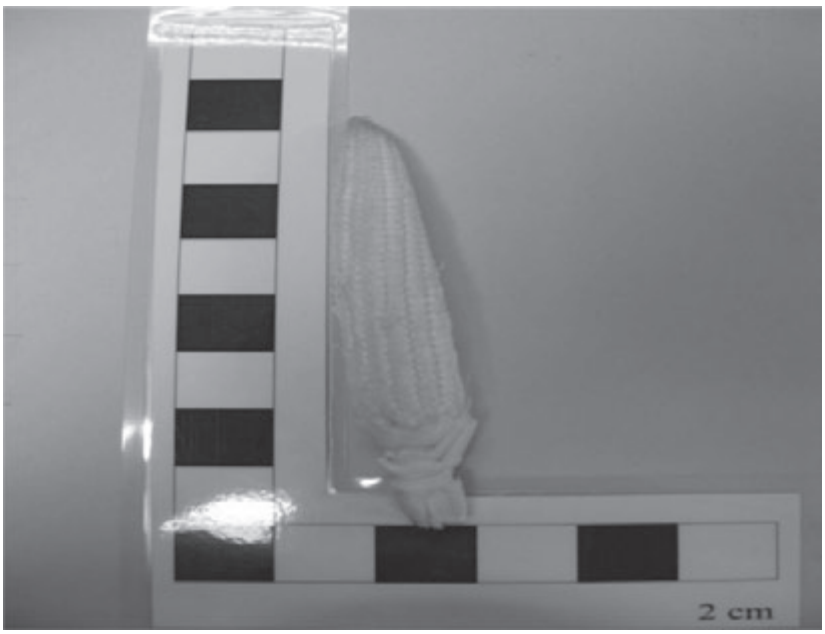

Fig. 1. Young corn ear

Fig. 2. Is an electron photomicrographs at low magnification (15-100X) of the young corn kernel. The sample ware dried without any treatment. From the horizontal section, pith (pt) is shown as (a) in Fig. 2. The pith region of corn stems is basically made up of large cells surrounded by a lignified primary cell wall with variable numbers of inner vascular bundles dispersed among them (Hatfield and Chaptman 2009). The pith cells are a defined shape, and positioned in the centre of corn kernel and adjacent to the xylem cell wall. The cotyledons seen in longitudinal section appeared circumferentially oriented. A single cotyledon (Fig. 2b.) is clearly shown with all the important features including testa (Ts), pericarp (P) and pedicel (Pe). This is in agreement with research done by others (Carpita *et al*. 2001).

Fig 2c. show the structure of the pedicel (Pe) where they are closely bound to cell membranes by febrile substances and connected with each other by long, hyphae-like strings (Goyal and Srivastava 2009). The root of corn silk also can be found in this area. In the photomicrographs examined, hair-like filaments appears in cross-section. The filaments with large numbers of

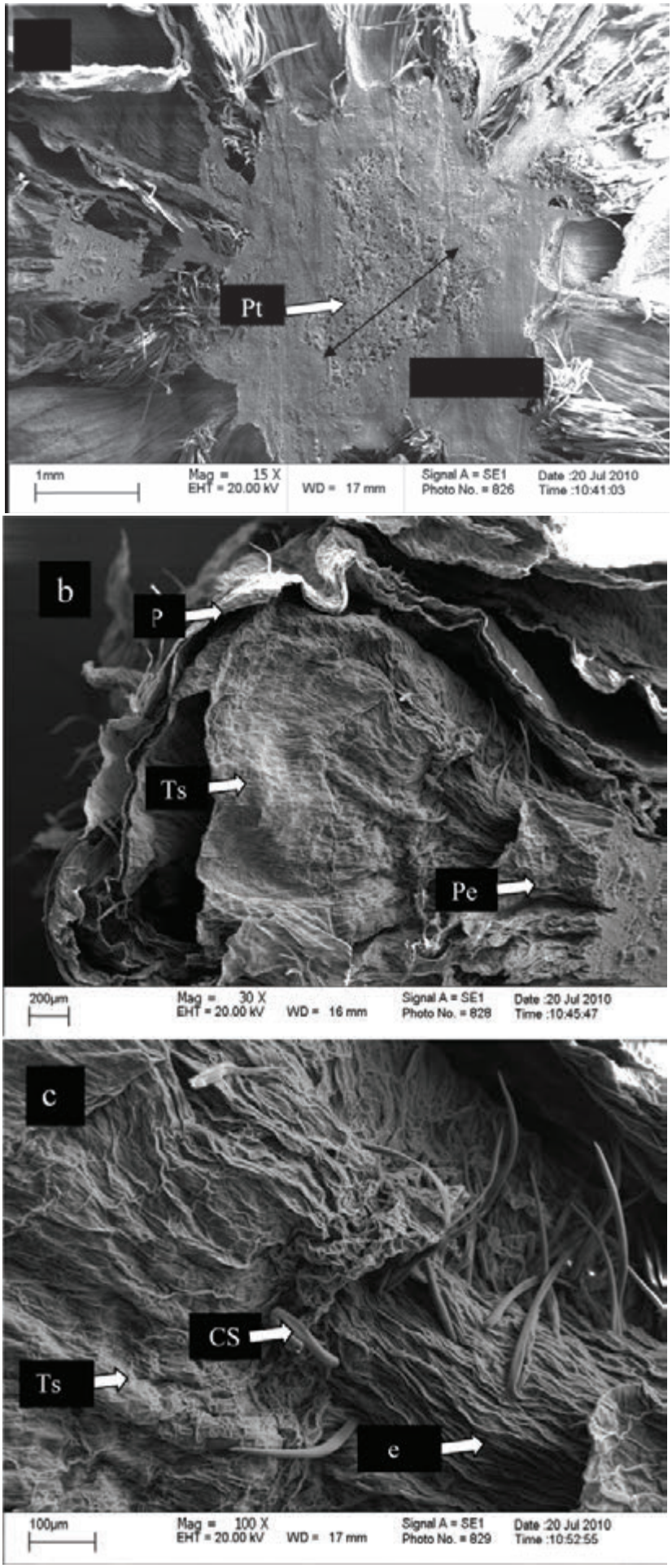

Fig. 2. (a,b,c) are scanning electron photomicrographs in low magnification (15-100X) of young corn ears. Photomicrographs 2a is representative of cells from young corn ears dried without any treatment in a horizontal section showing the pith (Pt) located at the centre of the kernel 15X. Photomicrograph 2b shows a single cotyledon with testa (Ts) pedicel (Pe) and pericarp (P). Photomicrograph 2c showing pedicel (Pe) and root of corn silk (CS) of the cotyledon at 100X.

prominent thin, but uniform structure suggest that it belongs to a meristematic root cell of the corn silk. The basis for this undeterminate corn silk growth is unknown. One possible mechanism is that it is controlled by the meristem alone, in which case meristematic cells are developmentally restricted to particular fates (Irish and Nelson 1988). Thus, the pedicel is the origin of corn silk or if the development of corn grains or cotyledon are the directive the formation of these structures persist. Where the directive comes from is conjectural. It may well be hormonal (abscisic acid or auxin) in nature as not all of the corn cobs in a particular plant form the baby corn at the time of maturity.

Table 1 Tabulation of the size of the baby corn ears freshly dried and post-treated by NaHClO

Features	Fresh Dried	NaHClO
Cotyledon size (mm)	1.8-2.5	1.6-2.0
Corn silk size (μm)	15-20	15-20
Pith diameter (mm)	1.55-1.65	1.45-1.55

Size is average of three readings

Fig. 3 (a,b,c) shows scanning electron photomicrographs of representative cells from young corn kernel treated with 4.5% sodium hypochlorite solution. The solution was used as a bleach to wash out the epidermis layer of the sample. The pith shows hexagonal scaffolding structure forming the majority of the space, here seen in low magnification (15-100X). The morphology of pith (Pt) is shown in Fig. 3a. It contains mostly of undifferentiated cells, usually large thin-walled parenchyma cells. The cells at the outer layer of the cortex often acquire irregularly thickened cell walls, and are called collenchymas cells (Russell and Evert 1985). The epidermis layer of the cotyledons structure perished upon treatment with sodium hypochlorite. The testa (Ts) is here seen exposing the endosperm (Fig. 3b.). This endosperm is a tissue that nourishes the embryo (Charlton *et al*. 1995). *Zea mays* being monocotyledon have a helobial endosperm, during an endosperm formation, the cell-wall formation coincide with nuclear divisions. In helobial endosperm formation, a cell wall is laid down between the first two nuclei, after which one half develops endosperm along the cellular pattern and the other half along the nuclear pattern (Carpita *et al*. 2001). The root of corn silk also can be found in this area. Fig. 3c elucidates the analogous structure made from single pith (Pt) in the cortex cell wall. These made up of three to four layers of sclerenchyma cells called hypodermis.

The size of the baby corn ears post-treated with 4.5% sodium hypochlorite solution decreases in size due to the destroyed epidermis layer of cotyledon. Corn silk size and pith diameter, nonetheless, doesn't have any significant changes.

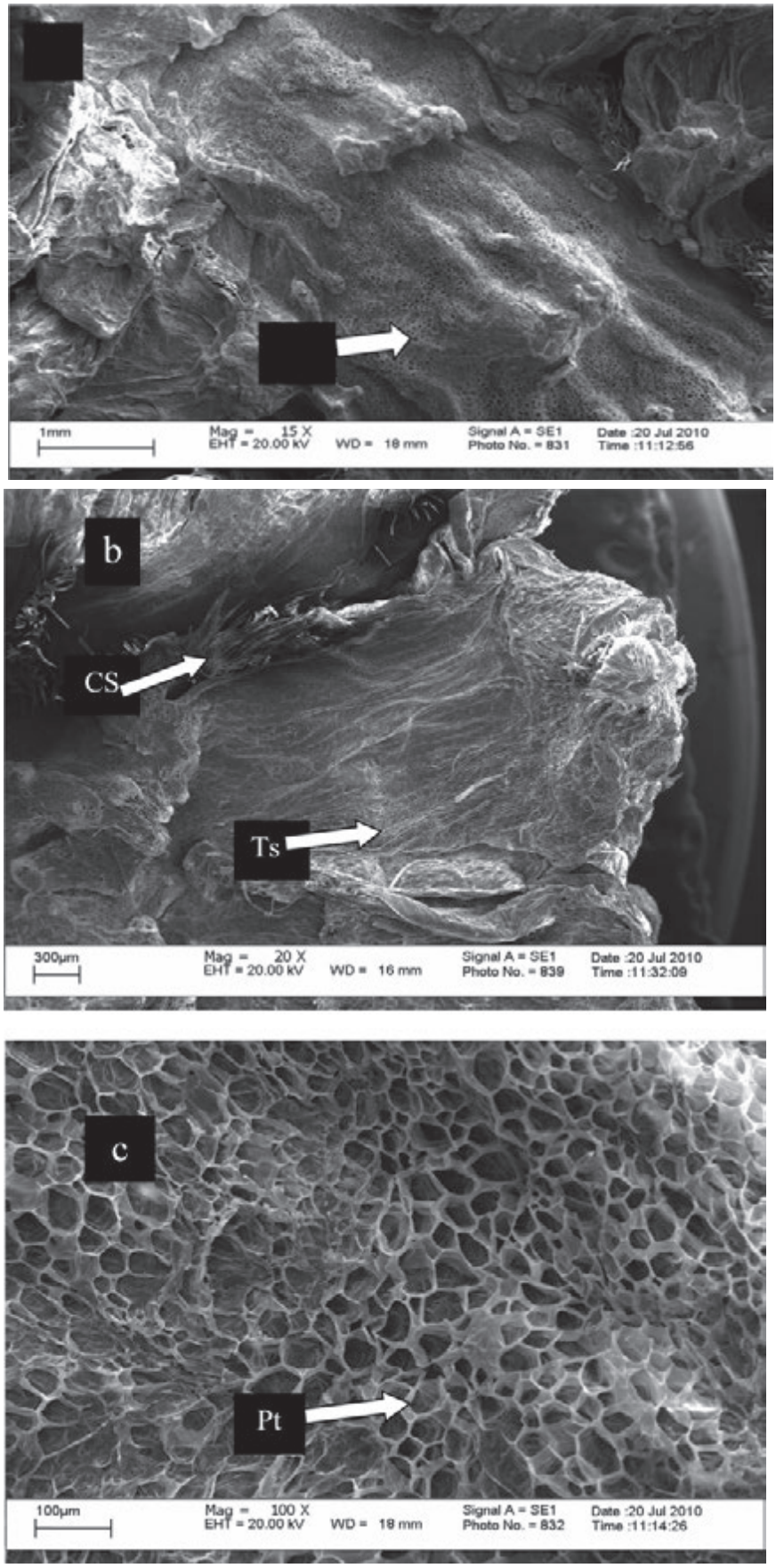

Fig. 3. (a,b,c) are scanning electron photomicrographs in low magnification (15X-100X) of young corn ears. Photomicrographs 3a representative cells from of the young corn kernel treated with 4.5% sodium hypochlorite solution from horizontal section showing pith (Pt) region located centre of the kernel 15X. Photomicrograph 3b shows a single cotyledon showing corn silk (CS) and testa (Ts) of cotyledon 30X. Scanning electron photomicrograph 3c shows the analogous structure of single pith (pt) in the cortex cell wall 100X.

Figure 4 (a,b) shows electron micrographs in high magnification (2000X) of representative corn silk from young corn kernel dried but without any treatment. Fresh corn silk threads from the matured corn sample were measured. The diameter ranges from 654 – 627 μm (Wan Rosli et al. 2007) while the size of these corn silks strands vary between 6-8 μm in diameter. Cross section of fresh young corn silk sample shows a single hollow tubular microtubule strand with longitudinally-oriented array tubes at every pedicel showing variability in size. The surface texture of the corn silk thread filaments was silky and smooth. Each one of them emanates from a single surface cell to increase the area of pedicel. The filaments with large numbers of prominent thin, but uniform structure is suggesting that it belongs to a meristematic root cell of the corn silk. The basis for this determinate corn silk growth is unknown. One possible mechanism is that it is controlled by the meristem alone, in which case meristematic cells are developmentally restricted to particular fates.

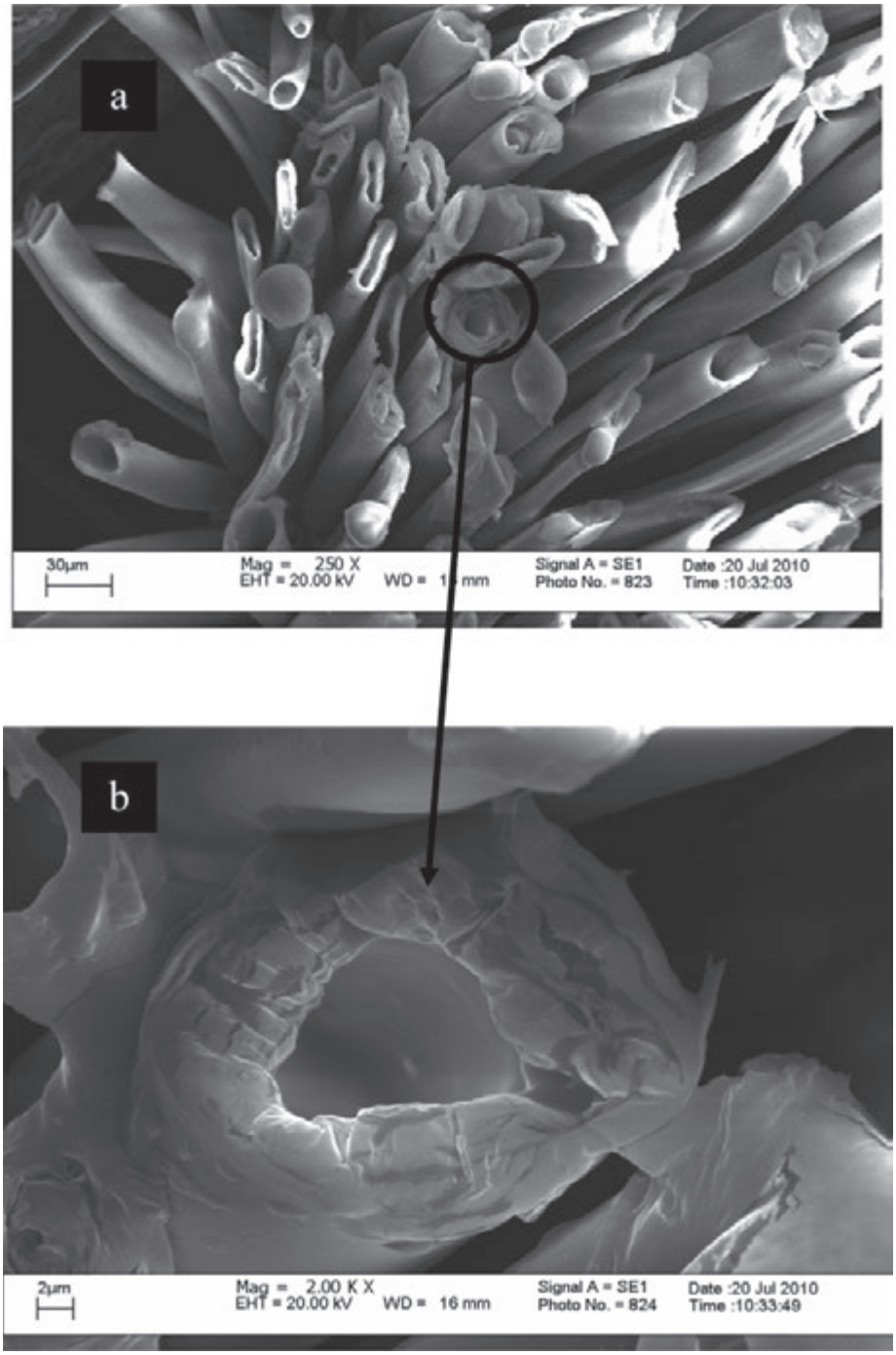

Fig 4 (a,b) are scanning electron photomicrographs in high magnification (2000X) of representative corn silk from of young corn kernel dried without any treatment.

CONCLUSION

The scanning electron microscope survey of the baby corn ears shows that there is a well developed organisation of structures conferring integrity to the baby corn. While at the same time interesting structures revealing the nature of corn silk together with baby corn may show evidence that the development of corn silk and mature corn could be controlled by some undetermined element probably hormonal in nature. This mean the formation of baby corn could be to ensure nutrient are directed to the dominant cob and this remain to be analysed further. Thus, the structures observed under SEM are showing a well developed architectural design giving the young corn strength. However, the reason why the corn plant produce baby corn, in the first place need further evaluation.

ACKNOWLEDGEMENTS

The authors would like to acknowledge the Universiti Sains Malaysia's short term grant number 304/PPSK/61310056 funding of this research undertaking. Special thank to Mr. Saiful Haizad Ahamad Jainid and Mr.Jamaruddin Mat Asan from the School of Health Sciences, Health Campus, USM and also the staff of Electron Microscopy Unit of Universiti Putra Malaysia, Institute of Biosains, for their technical assistance and support.

REFERENCES

Almeida, I. P. d. C., Silva, P. S. L. e., Negreiros, M. Z. d. and Barbosa, Z. 2005. Baby corn, green ear, and grain yield of corn cultivars. *Horticultura Brasileira* 23:960-964.

Amesz, J., Hoff, A. J., Boekema, E. and Rögner, M. 2004. Electron Microscopy. Pages 325-336-336 in Govindjee, ed. Biophysical Techniques in Photosynthesis. Springer Netherlands.

Bar-Zur, Schaffer, A. and A. 1993. Size and Carbohydrate Content of Ears of Baby Corn in Relation to Endosperm Type (Su, su, se, sh2). *J. American Society for Horticultural Science.* 118 (1):141.

Carpita, N. C., Defernez, M., Findlay, K., Wells, B., Shoue, D. A., Catchpole, G., Wilson, R. H. and McCann, M. C. 2001. Cell Wall Architecture of the Elongating Maize Coleoptile. *Plant Physiology* 127(2):551-565.

Charlton, W. L., Keen, C. L., Merriman, C., Lynch, P., Greenland, A. J. and Dickinson, H. J. 1995. Endosperm development in Zea mays; implication of gametic imprinting and paternal excess in regulation of transfer layer development. *Development* 121(9):3089-3097.

Chutkaew, C. and Paroda, R. S. 1994. Baby corn production in Thailand—a success story. FAO Regional Office for Asia & the Pacific, Asia Pacific Association of Agricultural Research Institutions,APAARI Publication 1994/1:20pp.

Goyal, P. and Srivastava, S. 2009. Characterization of novel Zea mays based biomaterial designed for toxic metals biosorption. *J. of Hazardous Materials* 172(2-3):1206-1211.

Hatfield, R. D. and Chaptman, A. K. 2009. Comparing Corn Types for Differences in Cell Wall Characteristics and p-Coumaroylation of Lignin. *J. Agricultural and Food Chemistry* 57(10):4243-4249.

Irish, E. E. and Nelson, T. M. 1988. Development of maize plants from cultured shoot apices. *Planta* 175(1):9-12.

Lund, H. A., Vatter, A. E. and Hanson, J. B. 1958. Biochemical and Cytological Changes Accompanying Growth and Differentiation in the Roots of Zea mays. *J. Biophysical and Biochemical Cytology* 4(1):87-98.

Russell, S. H. and Evert, R. F. 1985. Leaf vasculature in Zea mays. L. *Planta* 164(4):448-458.

S.Kasikranan, Jones, H. and Suksri, A. 2001. Growth, Yield, Qualities and Appropriate Sizes of Eight Baby Corn Cultivars (Zea mays L.) for Industrial Uses Grown on Oxic Paleustults Soil,

Northeast Thailand. *Pakistan J. of Biological Sciences* Vol: 4(Issue: 1): 32-36.

Wan Rosli, Jesmine, Mohsin and Farid. 2007. Variable pressure scanning electron microscopy (VPSEM) and Atomic absorption spectrometer characterization of *Zea mays* (Maydis stigma) hairs. A revisit to harness tangible therapeutic prowess. *Proceedings of the 6th ASEAN Microscopy Conference*.

Visualization of Clay in Pencil Core Using SEM-EDX

Pornpot Nuthong*
Scientific Equipment Center, Prince of Songkla University, Songkhla, Thailand
**Corresponding author: Email: pornpot.n@psu.ac.th*

ABSTRACT

The microstructure and elemental composition of pencil core containing different level of clay with varying hardness were analyzed by scanning electron microscopy (SEM) and energy dispersive X-ray spectrometry (EDX). Based on the fracture surface morphology, all samples had rough surface. EDX result revealed that all samples consisted of carbon (C), oxygen (O), aluminum (Al), silicon (Si), potassium (K), calcium (Ca) and iron (Fe). The contents of four elements (C, O, Al and Si) were formed to determine the hardness of pencil core. Hardness generally increased with increasing Al and Si contents. Distribution of elements visualized using X-ray mapping images confirmed the different contents of those elements. Sample with low hardness possessed high C content. Therefore, these analytical techniques can be used to differentiate the hardness of pencil core which contained varying contents and types of elements.

Keywords: Clay; Pencil core; SEM; EDX

INTRODUCTION

Clay minerals are the essential constituents of argillaceous rocks. Clays are widely used in the production of food, feedstuffs, beverages, paper, rubber, plastics, artificial leather, protective coating, pharmaceutics, cosmetics, paints, pencil, pastels, porcelain, electro-porcelain and other fine ceramics and sialon ceramics (Konta, 1995). Generally, clays are mixed and blended to give standard composition and optimum properties for various applications (Rossman and Carel, 2002). Several types of clays contain different clay minerals of the ninety-three planar/non-planar hydrous phyllosilicates which are either 1:1 or 2:1 layer type phyllosilicates with/without interlayer water (Haq *et al.,* 2009). The chemical composition of clays composed essentially of silica, alumina and water (Grim, 1968).

Graphite is a polymorph of the element carbon. It is abundantly available as coal or as natural graphite. The graphite crystal lattice consists of stacks of parallel two dimensional graphene sheets with sp^2 hybridized carbon atoms tightly bonded in hexagonal rings (Sengupta *et al.,* 2010). A graphite pencil consists of a writing core (or lead) and a protective casing (made of wood). Lead of pencil contains a mixture of graphite, clay and wax. Clay is the important component used in making and classifying the pencil lead. The degree of hardness and softness is the importance aspect of the lead. Pencil hardness is classified nineteen degrees ranging from 9H to 8B (Sousa and Buchanan, 2000).The hardness of the lead depends on the percentage amount of graphite and clay. The hardness of pencil lead increased with increasing amount of clay. Grade HB contain about 65% graphite by weight and the remnant clay (Blau and Gardner, 1996).

The characterization and discrimination of pencil lead, utilizing high power microscopy (Cain, 1978), X-ray fluorescence spectrometry (XRF) (Cain, 1978), Mass spectrometry (Zoro and Totty, 1980), time-of-fight secondary ion mass spectrometry (ToF-SIMS) and inductively coupled plasma mass spectrometry (ICP-MS) (Denman *et al.,* 2007), have been reported. Cain et al. (1978) compared the elemental composition of pencil core using XRF. They found that the peak ratio of calcium/iron and potassium/iron could be used to distinguish between samples. Zoro and Totty (1980) applied the mass spectrometer in analyzing pencil cores for discriminating between manufacturers. The quantitative data analyzed by Denman et al. (2008) showed that the application of ICP-MS and ToF-SIMS in analyzing HB pencil cores could be used to differentiate between manufacturers. They concluded that the analysis of a trace amount of pencil marking has

a similar power of discrimination to that of bulk analyses.

From the previous literature could be concluded that there is scope to differentiate pencil leads on the elemental composition. However, no information regarding elemental localization and distribution of the basis of lead elemental ingredient has been reported. The aim of the present study was to characterize and discriminate the pencil lead with different hardness degree using scanning electron microscopy (SEM) and energy dispersive x-ray spectrometry (EDX). The elemental composition and morphology of pencil lead with difference hardness degree are presented.

MATERIALS AND METHODS

Pencil lead preparation

Pencil was purchased from STAEDTLER (Bangkok, Thailand). 6 hardness degrees (5H, 2H, HB, 2B, 4B and 6B) of pencil lead were used. After lead was removed from the wood casing by the cutter, there was broken with hand.

Scanning Electron Microscopy (SEM)

The fracture surface of pencil lead was mounted on the brass tub with carbon tape. Morphology of pencil lead was observed using a scanning electron microscope (JSM-5800LV, JEOL, Japan) operated at an accelerating voltage of 20 kV with the magnification of 500x.

Energy Dispersive X-ray Spectrometry (EDX)

The chemical analysis of pencil lead was studied by energy dispersive x-ray spectrometer (ISIS300, Oxford, England) performed at an accelerating voltage of 20 kV with high vacuum mode. The element concentration of carbon, oxygen, aluminum and silicon were used to compare and differentiate between the hardness degrees of pencil lead. The distribution of each element in the sample was obtained with elemental mapping analysis mode. Elemental mapping images were captured after a hundred frames of mapping were recorded with the magnification of 500x.

Statistical Analysis

Data were subjected to analysis of variance (ANOVA) and mean comparisons were carried out by Duncan's multiple range test (Steel and Torrie, 1980). Analysis was performed using the SPSS package (SPSS 11.0 for windows, SPSS Inc., Chicago, IL, USA).

RESULTS AND DISCUSSIONS

SEM analysis

SEM micrographs illustrating the morphology of the fracture surface of pencil lead with different degrees of hardness are observed in Figure 1. The rough surfaces of leads were found in all samples. Nevertheless, clay particle and graphite could not be discriminated by SEM. The brittle of lead was found in high content utilization of graphite. Due to carbon atoms of graphite in each layer were bonded with strong covalent bonds, whereas between layers were connected by weak force that could be slide over each other in graphite. The fracture surface of lead at high hardness degree is denser (Fig. 1a and 1b) due to clay was incorporated in higher concentration. Thus, the amounts of clay and graphite were impacted to the morphology of fracture surface. The increment of clay content in pencil lead could improve the hardness of lead by combining with carbon atoms between graphite layers.

EDX showed that, the energy dispersive spectra of the X-rays character emitted the following elements of Carbon (C), Oxygen (O), Aluminum (Al), Silicon (Si), Potassium (K), Calcium (Ca), Titanium (Ti) and Iron (Fe) (Fig. 2). From the examinations C, O, Al and Si were the main elements used to compare pencil lead hardness degree. EDX analysis showed presence of varying amounts of peak intensity of C, O, Al and Si in lead with different hardness (Fig.2). When the hardness

degree of lead was increased, peak height of C was decreased. Contrast, the increment of peak height of O, Al and Si were obtained in same hardness degree. The elements of C, O, Al and Si were obtained and mapped using Link ISIS 300 program. X-ray mapping images which mapped the elemental composition and distribution of their elements were presented in Fig. 3. C element was highest content and mostly abundant distribution in lead of 6B (Fig. 3 f1). While the element of Al and Si was highest concentration and densely populated scattering in lead of 5H (Fig. 3 a3 and a4). The result from EDX indicated that the concentration and distribution of elements were different.

The semi-quantitative analysis of pencil lead by EDX is summarized in Table 1. High concentration of carbon was observed in all samples due to graphite component. The elements silicon, aluminum and oxygen are the main composition which present in the clay [9]. It was significant in carbon, aluminum and silicon content between hardness degree ($p<0.05$). The highest concentration of C was presented in lead of 6B, whereas, the element of Al and Si content were observed with the minimum in same hardness degree ($p<0.05$). These results corresponded to peak heights of C, Al and Si shown in Figure 2. At the hardness degree value lower than 2H no decrease in O content was observed. The elements in lower concentration may be detected due to other

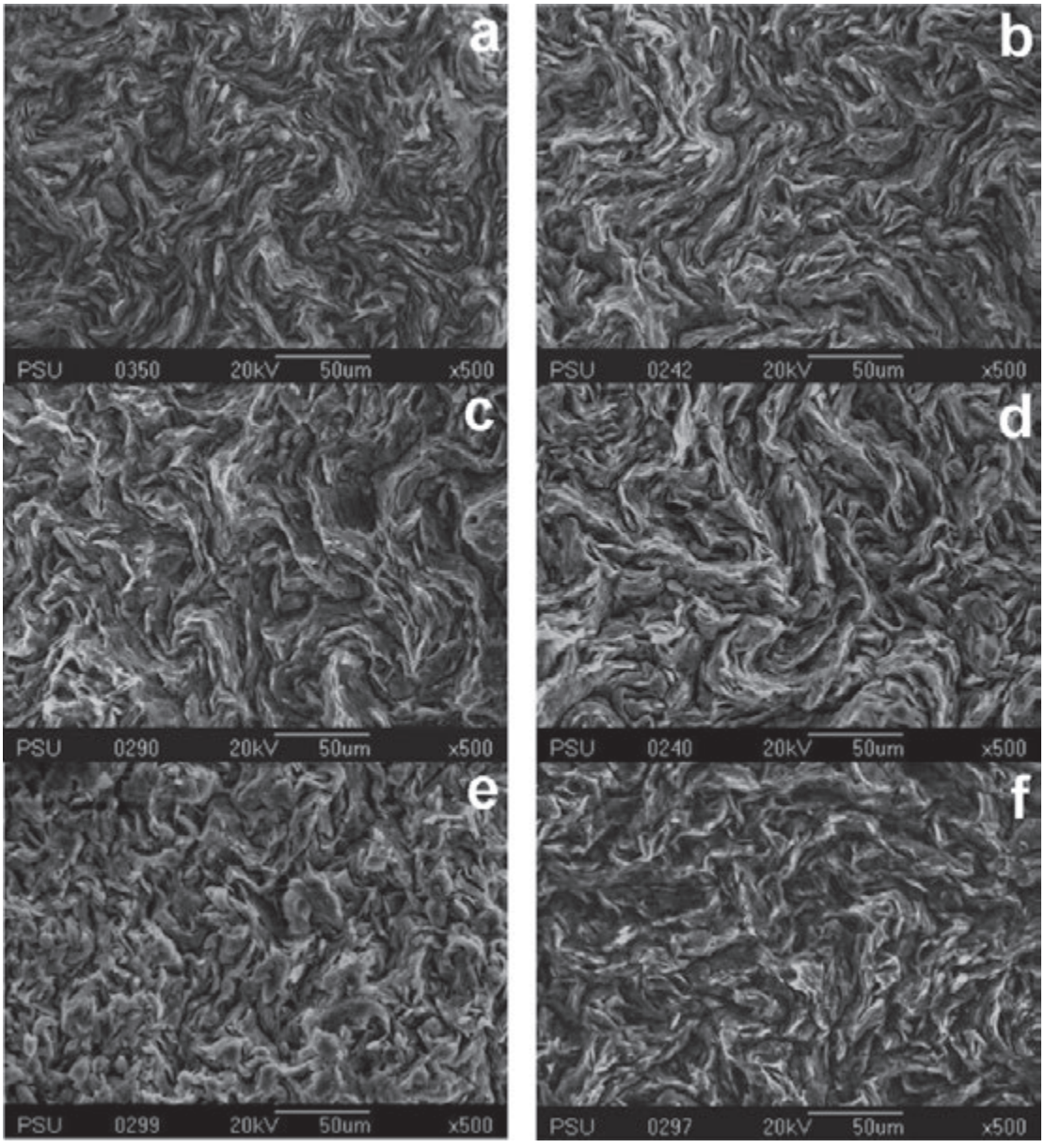

Fig. 1

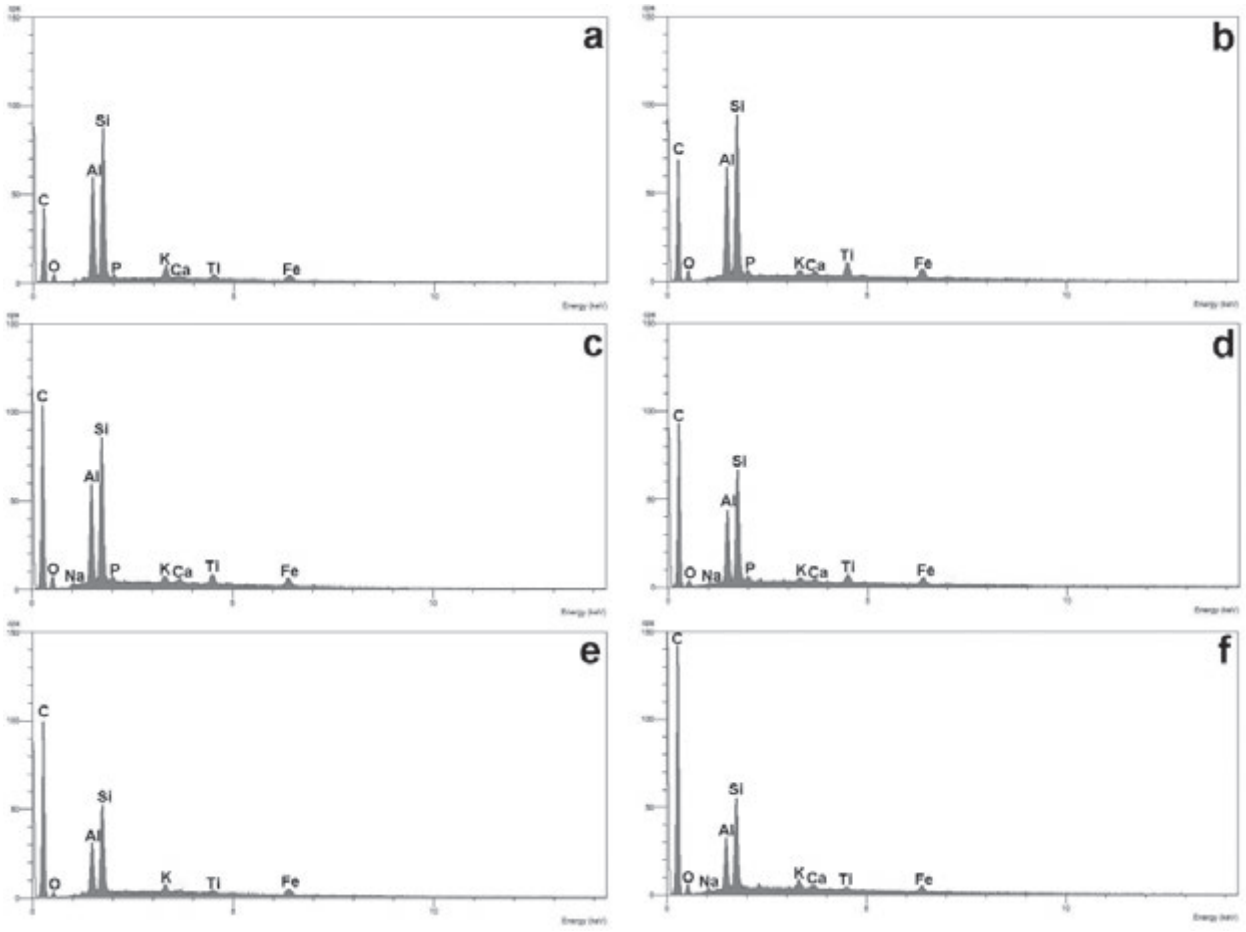

Fig. 2

clay ingredient (element not shown). Thus the comparison of the contents of C, O, Al and Si in 6 hardness degrees were usful to discriminate the pencil lead.

CONCLUSIONS

The morphology of fracture surface could not be used to discriminate the hardness degrees of pencil lead. Element of carbon, aluminum and silicon were used as a basis elements for discriminating between hardness degrees of lead. The elemental mapping technique appears to show the power to identify the distribution of specific elements present in the leads, especially, clay particles that were mixed in the lead containing aluminum and silicon and could not reveal by SEM. Thus, EDX can successfully be used to identify the hardness degree of pencil lead differentiated by elemental composition and distribution. The obtained information would be the fundamental data for forensic science study such as in the identification of pencil marking on paper.

ACKNOWLEDGEMENTS

This work is supported by Scientific Equipment Center, Prince of Songkla University, Hat Yai, Thailand.

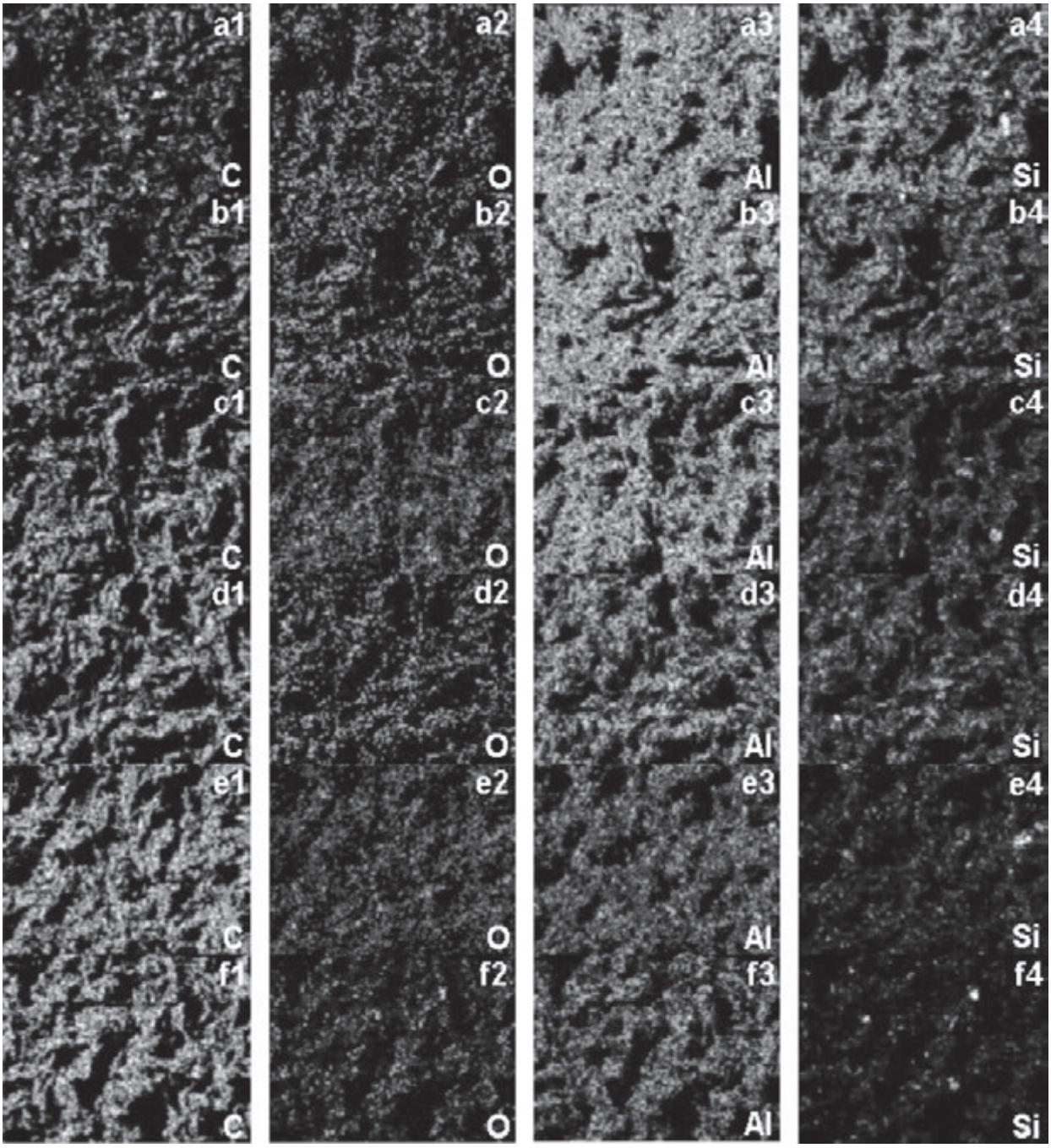

Fig. 3

REFERENCES

Blau P.J, Gardner J.K (1996) Tribological characteristics of graded pencil cores on paper. *Wear* 197: 233-241.

Cain S, Cantu A.A, Brunnelle R, Lyter A (1978) A scientific study of pencil lead components. *J. Forensic Sci.* 23: 643–661.

Denman J.A, Kempson I.M, Skinner W.M, Kirkbride K.P (2007) Discrimination of pencil markings on paper using elemental analysis: an initial investigation. *Forensic Sci. Inter.* 175: 123-129.

Grim R.E (1968) Clay Mineralogy. McGraw-Hill Book Company, New York.

Haq A, Iqbal Y, Khan M.R (2009) Phase and microstructural characterization of kaolin clays from north western Pakistan. *J. Pak Mater Soc.* 3: 77-90.

Konta J, (1995) Clay and man: Clay raw materials in the service of man. *App. Clay Sci.* 10: 275-

335.

Rossman F.G, Carel J.V.O (2002) Colloid and surface properties of clays and related minerals. Marcel Dekker Inc., New York.

Sengupta R, Bhattacharya M, Bandyopadhyay S, Bhowmick A.K (2010) A review on the mechanical and electrical properties of graphite and modified graphite reinforced polymer composites. *Prog. Pol. Sci.* 36: 638-670.

Sousa M.C, Buchanan J.W (2000) Observation models of graphite pencil materials. *Computer graphics forum*. 19: 27-49.

Steel R.G.D, Torrie J.H (1980) A biometrical approach: principles and procedure of statistics. McGraw-Hill, New York.

Zoro J.A, Totty R.N (1980) The application of mass spectrometry to the study of pencil marks. *J. Forensic Sci.* 25: 675–678.

Cytological and Cytochemical Studies on the Pulmonary Alveolar Macrophages of the Rat "*Rattus rattus norvegicus albinus*"

Mohammad O. Salman[1], Ali H. Abd [1], Imad M. Al-Ani[2*] and Anam R. Al-Salihi[3]
[1]*Department of Human Anatomy, College of Medicine, Al-Nahrain University, Baghdad, Iraq.*
[2]*Department of Basic medical Science, Kulliyyah of Medicine, International Islamic University Malaysia, Kuantan, Malaysia*
[3]*Institute of Embryology Research & Infertility treatment, Al-Nahrain University, Baghdad, Iraq.*
[*]**Corresponding address:** *Tel. +60179776014. E-mail imad_alani@yahoo.com*

ABSTRACT

The objective of the present study was to find the normal values of the cytology and cytochemistry of the Pulmonary Alveolar Macrophages (PAMs) and through the identification of universal normal values. Bronchoalveolar lavage (BAL) fluid was performed by tracheal cannulation to seventy healthy adult male rats. The percentages of differential BAL cells count were 85-90% PAMs, 5-6% lymphocytes, 3-4% granulocytes and 3-4% epithelial cells. The diameter of PAMs was ranging between (14-35µ). The mean of PAMs area was 57µ2±1.03. The mean of nucleus area was 17.6µ2±1.3. The ratio of nucleus areas to cytoplasm area was1:2. The Final Reaction Product of the ANAE was homogenous brown reddish color. It was homogenous in distribution although the distribution was regular within the area of cytoplasm and nucleus of PAMs while other BAL cells showed negative reaction. 95% of total PAMs were positive in reaction. The mean of optical density of final reaction product of esteratic activity in PAMs was 1.782±0.004.

Keywords: Pulmonary Alveolar Macrophages, Bronchoalveolar lavage, Optical density, Tracheal cannulation, Final reaction product

INTRODUCTION

Pulmonary alveolar macrophages (PAMs) are a type of macrophages found in the pulmonary alveoli, near the pneumocytes, but separated from the wall; they play a critical role in homeostasis, host defense, the immune response to foreign invaders, and tissue remodeling (Lambrecht, 2006). They also release substances that stimulate other cells of the immune system, thus are involved in cell-mediated immune responses (Rao *et al.,* 2002). Alveolar macrophages contain the polysaccharidase lysozyme, which digests the walls of many bacteria. A peroxidase is involved in the bactericidal activity of monocytes, but the enzyme is absent in tissue macrophages (Paul *et al.,* 2002).

Morphologically the PAMs are variable owing to their metabolic versatility and rapid adaptability in responding to infective challenges (Oliver *et al.,* 2003). PAMs ingest solids or liquids by microendocytosis, a ruffled membrane is characteristic of cells active in endocytosis and a smooth membrane characteristic of quiescent ones (Ganz *et al.,* 1985). In quiescent PAMs, the agranular endoplasmic reticulum predominates over the granular, but the latter increases dramatically in volume shortly after cells become stimulated to produce lysosomal enzymes, antibacterial secretions like lysozyme, interferon, and components of complement, or other substances synthesized in bulk (Riott *et al.,* 1998).

Bronchoalveolar lavage (BAL) is a diagnostic procedure in which a bronchoscope is passed through the mouth or nose into the lung and physiological saline fluid is squirted into a small part of the lung and then recollected for examination. BAL is commonly used to diagnose lung diseases in people with immune system problems, (Henderson, 1994). Cellular and non-cellular components are flushed out of the alveoli by BAL and are hence rendered accessible to diagnosis (Jeffrey et al., 1995).

Analysis of the lavage fluid may give some insight into the nature and degree of dust exposure

(Dethloff *et al.,* 1987). BAL fluid differential cell counts evaluate the diagnostic impact of the pulmonary alveolar macrophages (PAMs) and lymphocytes (De Brauwer *et al.,* 2000).

The present study was carried out to investigate the normal cytological features and values of PAMs using quantitative study of BAL procedure and demonstrate the usefulness of differential cell counts of BAL.

MATERIALS AND METHODS

Animals

Seventy healthy adult male *Rattus rattus norvegicus albinus* rats, (25 weeks old weighting "300 ± 50 g"), were kept under suitable environmental conditions such as a room temperature that was maintained at about (24±2)°C and exposed to 12 hour/day light program.

Experimental Design

The animals were divided into four groups. Group 1; 10 rats used for cytological characterization and differential BAL count. Group 2; 10 rats used for PAMs count. Group 3; 20 rats used for morphmetric study and Group 4; 30 rats used for cytochemical study to identify Alpha naphthyl acetate esterase "ANAE" activity.

Each animal was anesthetized with single intraperitoneal dose of 0.2 ml of Ketamine (Hyprochloride) (50 mg/ml) (OUBARI PHARMA-Helepo-Syria) and 0.05 ml Xylazine (Rompun 2%) (23.32 mg/ml) (OUBARI HARMA-Helepo-Syria). Animals were sacrificed by exsanguinations without cutting tracheal muscle to insert the metal tube that was ligated by suture material for tracheal cannulation.

The bronchoalveolar lavage BAL was performed by tracheal cannulation and a total volume of 48ml phosphate-buffered saline (PBS; pH 7.4) was installed in 8ml aliquots for 20 sec. The thorax was gently massaged throughout this procedure.

The differential BAL cells count was performed using of Geimsa's stained BAL smears. Ten slides were chosen randomly from Group 1, "1 slides form each rat". 400 cells were counted from peripheral area of each slide. From each animal about 20 slides were prepared and stained with H&E stain. Then, one slide randomly selected from each animal slides and 100 PAMs were chosen.The system is designed especially for scientific analysis of a given image obtained by an external source (a digital capture camera) by which different processing or procedures can be performed.

The esteratic activity against the substrate α-naphthyl acetate was demonstrated according to the azo coupling method of (Al-Salihi, 1986) and its modifications as detailed by (Oliver *et al.,* 1991). To obtain the required wave length for a particular measurement an automatic wave length scan using interference wedge filter in the range 400-700 nm was employed. The determination of the wavelength of maximal absorbance of the final reaction product of a particular enzyme was done by wavelength scan module of the polyspec Desktop Spectrometer.

RESULTS

The fluid recovered by the BAL technique applied in this study contained all BAL cells, including; lymphocytes, granulocytes and epithelial cells (Figure -1).

The recovered volume was ≈ 44 ml from total 48 ml. The lavage fluid was installed in 8ml aliquots for 20 sec. Usually 4-6ml was recovered upon first 8ml installation while with the consequent recovered lavages was 7.5-8ml (92% of total lavage fluid was recovered).

The Giemsa stained smears revealed the cytological criteria of PAMs. These criteria were identical to those obtained by the H&E staining; including the rounded shaped cells, the morphological and numerical variability of the PAMs nuclei. The nuclear–cytoplasm demarcation was less clear with Giemsa staining (figure -2).

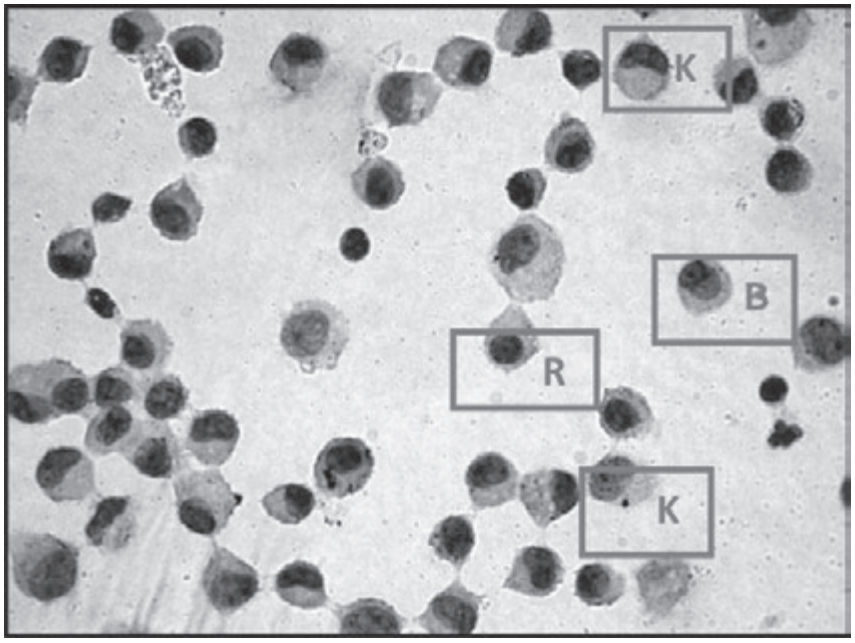

Fig-1: BAL smear illustrating the cell types and morphologies Numerates PAMs are seen. Nuclei of PAMs are rounded (R), idney (K) shaped and i-nucleated (B). Cytoplasm is pink in color (H&E stain).X1000).

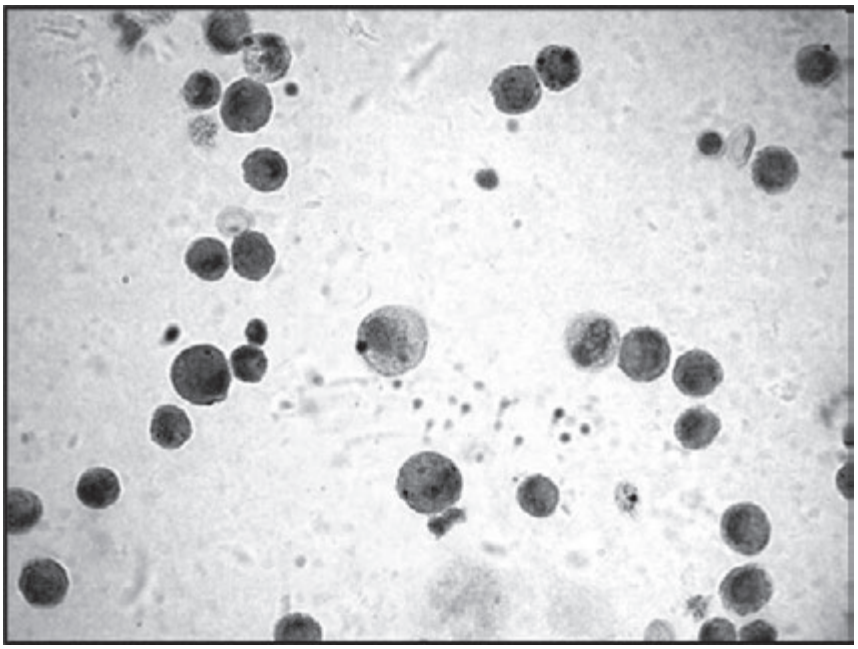

Fig-2: BAL smear stained with Giemsa stain. The nucleo-cytoplasmic demarcation of the PAMs is not sharp. X1000

The mean of total cells counted from recovered lavage fluid was 2.6×10^6 cell /animal. The percentages of differential BAL cells count were composed of 85-90% PAMs, 5-6% lymphocytes, 3-4% granulocytes and 3-4% epithelial cells. PAMs were easily distinguished from other BAL cells by their morphological features.

The present study showed that: 350 ± 0.4 cells were PAMs and ranged between 355-382 PAMs, lymphocytes 22 ± 0.23, granulocytes 12 ± 0.35 and epithelial cells 15 ± 0.44 (Table -1).

Table -1: Differential cells count of BAL.

Cells types	Total cells count (mean ± SD)	Cells Percentage%
PAMs	350 ± 0.40	85-90%
Lymphocytes	22 ± 0.23	5-6%
Granulocytes	12 ± 0.35	3-4%
Epithelial cells	15 ± 0.44	3-5%

A total of 2000 PAMs were analyzed in the 20 slides prepared for the morphometric study. Frequency distribution test was administrated to the areas of each PAM, the PAMs nuclei and cytoplasm. The diameter of PAMs ranged between (14-35μ).

The mean of PAMs area was 57±1.0 μ2; ranged from 28.2–96.9μ2, the mean of nucleus area was 17.6±1.3 μ2; ranged from 7.43–31.3 μ2 and the mean of cytoplasm area was 39.1 ± 0.8 μ2; ranged from 15.7–73.6 μ2. The ratio of nucleus areas to cytoplasm area was approximately 1:2 (Table -2).

Table -2: the statistical analysis of PAMs area (μ2) and nuclear area (μ2)

Measurement	Cell area (μ2)	Nuclear area (μ2)	Cytoplasm area (μ2)
Mean ± SD	57 ± 1.0	17.6 ± 0.4	39.3 ± 0.7
Median	55.8	17.1	38.8
Mode	47.8	18.8	42.9
Range	68.7	23.9	63.9
Minimum	28.2	7.4	15.7
Maximum	96.9	31.3	79.6

The results of the final reaction product of the ANAE enzymatic reaction was homogenous brown reddish color. The cytoplasm and nucleus of PAMs showed regular and homogenous brown reddish color distribution, however; other BAL cells showed negative reaction (figure -3).

The optical density (O. D.) was measured in cytoplasm through measuring the transmittance, according to the formula (section 2.6.1) value of the final reaction product of pulmonary alveolar macrophages ANAE in group of 100 PAMs, the mean of O. D. of ANAE activity in measured PAMs was 1.782±0.004, ranged between 1.67–1.91; the microspectro–photometric data and statistical analysis of O.D. were shown in (table -3). The frequency distribution of the microspectrophotometric data is shown in the form of histograms (figure -4) for ANAE cytochemical activity.

DISCUSSION

Bronchoalveolar lavage (BAL) is a safe, simple, and inexpensive technique that any equine Practitioner can perform, without sophisticated equipment or advanced skills (Mansmann and King, 1998). In the present study, the BAL procedure was administrated *in situ* and was found helpful to keep PAMs in a morphological feature similar to viable cells and to prevent any morphological and cytochemical deterioration.

BAL smears stained with H&E showed that PAMs were characterized by blue to dark blue nuclei and acidophilic cytoplasm with varying pink' shades, H&E has been used successfully

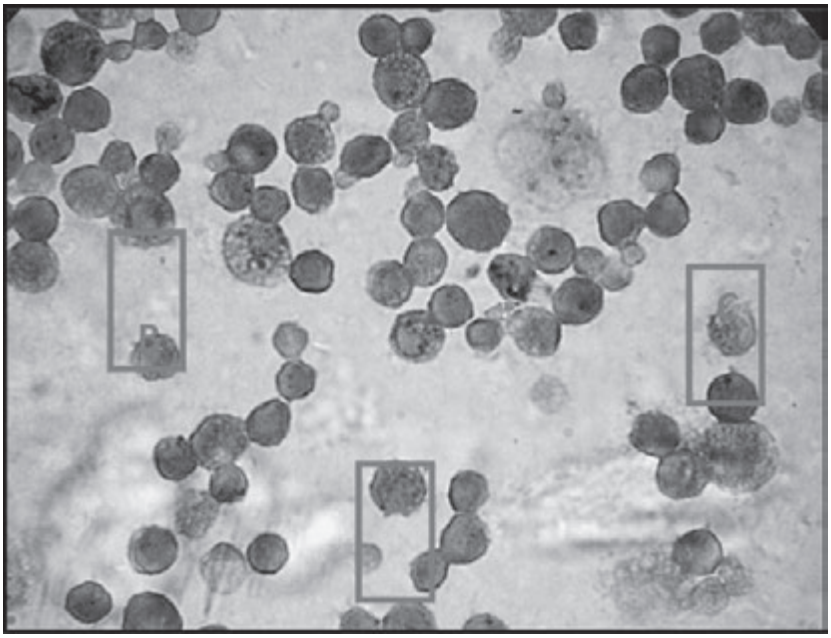

Fig-3: Esteratic activities in PAMs as demonstrated by alpha Naphthyl acetate. (A) PAMs show homogenous activity, (B) PAMs nuclear membrane and nucleus activity brown reddish color of final reaction product. In other BAL cells (C) show negative reaction. X1000

Table -3: The Optical Density O.D. values of the Final Reaction Product of ANAE activity and statistical analysis in group of 100 of PAMs.

Statistical analysis	value
Optical density mean	1.782
Standard error	0.004
Range	0.241
Minimum	1.669
Maximum	1.91
(PAM) count	100

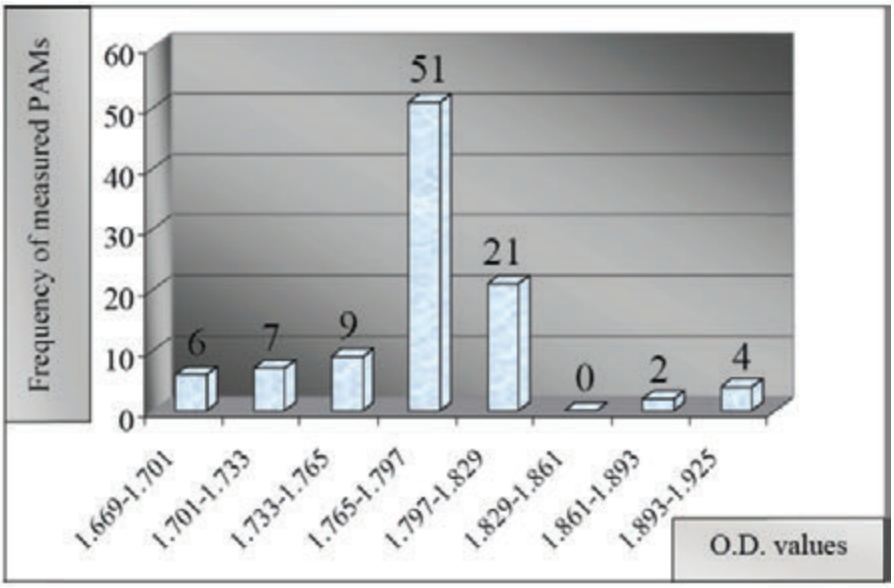

Fig- 4: Frequency distributions for O. D. of Final Reaction Product of ANAE activity in PAMs

for clear demarcation among the nuclei border, the cytoplasm and cell membrane of PAMs in BAL smears (Al-Obaidi 2006). The Giemsa stained slides of BAL smears clearly demonstrated the cytological features of the cells and therefore cells were easily differentiated into PAMs, lymphocytes, granulocytes and epithelial cells (Thompson *et al.,* 1996).

Using the "poly freehand" tool in this study, assists the measurements of PAMs slides borders of the area more precisely; the flexibility of the tool allowed borders to be set while avoiding the damaged or non-PAMs cells.

The diameters of PAMs were in the range of (14-35μ). Pugh *et al.* (1983) showed that the PAMs diameter was (10-16μ), Tetuo *et al.* (1997) identified the diameter of PAMs which ranged between (20-50μ). In their study on human PAMs, Ibrahim-Granet *et al.* (2003) showed that these cells were (10-13μ) in diameter, and Junqueira and Carneiro (2005) showed that the diameter was (10-30μ).

The average PAMs' count from the recovered lavage fluid calculated in this study from 10 male rats by morphological evaluation of cytological BAL smears preparation was 2.6×10^6 per rat. The differential cells count of BAL was very important to calculate the PAMs percentage among other cells; normally present in BAL smears. Four hundred cells from each BAL smear slide were counted. This number was not randomly selected, but it was the most acceptable number among various studies which used different methods for numbering the cells (Fleury *et al.,* 1985; Rehn *et al.,* 1992; Wisniowski *et al.,* 2000; Lasbury *et al.,* 2003). Differential cells count of BAL smears shows that: PAMs 85-90%, lymphocytes 5-6%, granulocytes 3-4% and epithelial cells (including squamous cells and columnar epithelial cells) 3-5%.

The present investigation is inconsistent with previous studies in different species; Laplante and Lemaire (1990) studied the migratory function of the alveolar macrophage in the male Wistar rats and found PAMS 90.2%, lymphocytes 0.7%, granulocytes 0.1% and epithelial cells 0%. Rehn *et al.* (1992) investigated the alveolar macrophages of female Wistar rats by bronchoalveolar lavage under normal and activated conditions and found PAMs 95%, lymphocytes 2%, granulocytes 3% and epithelial cells 0%. Khalil *et al*. (1993) examined the alveolar macrophages isolated from the female Sprague-Dawley rats and demonstrated the constitution consisted of PAMS 92%, lymphocytes 1.5%, granulocytes 5% and epithelial cells 1.5%. Lasbury *et al.* (2003) stated that counting of alveolar macrophages in the lavage fluids of female Sprague-Dawley rats revealed PAMs 98%, lymphocytes 2%, granulocytes 0% and epithelial cells 0%. These variations may be related to species difference or/and the physiopathological status of the animal used.

Cytochemical demonstration of carboxyl ester hydrolases in PAMs smears with α-naphthyl acetate esterase (ANAE) showed intense reactivity in the present study. The simultaneous coupling azo-dye was very efficient method used for the demonstration of these classes of esterase hydrolyzing naphthyl acetate (Al-Azzawi *et al.,* 1990; Al-Salihi *et al.,* 2002). Adequate localization of the enzymatic reaction of ANAE could be noticed; moreover the color characteristic is more easily identified and demonstrated at light microscopic study.

Esterase activity was used as PAMs' marker, for identification of PAMs among other BAL cells; the final reaction product appeared as a positive reaction in 95% of the total PAMs. The final reaction product of the ANAE enzymatic reaction was brown reddish in color. It was homogenous in distribution, although the distribution was regular within the area of cytoplasm and nucleus of PAMs while other BAL cells showed negative reactions. This result is consistent with the characterization of final reaction product results of human alveolar macrophage (Al-Doski, 1984; Jianmin *et al.,* 2004).

The use of hexazotized para roseaniline as coupling agent and α-naphthyl acetate as substrate in simultaneous azo coupling reaction is recommended for correlative quantization of esterases histochemically and biochemically. The wave length of maximal absorption is 425 nm (Al-Salihi, 2002).

Using a small measuring diaphragm that includes the cytoplasm only will collect light from all heterogeneous area of the cytoplasm which gaves an overall estimate of the intensity of the final

reaction product color and overcome the distributional error.

In present study, the optical density of final reaction product of ANAE activity in PAMs was measured; the mean of O. D. was 1.782 ± 0.004 and ranged between 1.669–1.910.

Previously, the description of ANAE activity that was applied subjectively depended on positive or negative reaction and was considered as one of the histochemical and biochemical quantitative measurements (Pugh *et al.,* 1983). ANAE analysis of cytochemical parameters in alveolar macrophages plays important part in the analysis of their relative contribution to the development of lung malignancies. (Zunic *et al.,* 1997). Formigli et al. (2001) used the ANAE to detect the presence of newly re-cruited macrophages within the ischemic and early postischemic myocardium.

CONCLUSION

The present study described the characteristic features of the rat' "*Rattus rattus norvegicus albinus*" alveolar macrophages and showed that this species is a suitable experimental animal for further studies related to respiratory diseases and malignancies using α-naphthyl acetate esterase, bronchoalveolar lavage , pulmonary alveolar macrophages, final reaction product and optical density.

REFERENCES

Al-Azzawi H T, Al-Salihi AR, Al-Sabti SA (1990). Nerve muscle interaction – possible role of carboxyl esterase in skeletal muscle fiber differentiation. *Kufa Medical J*. 2: 121-126.

Al-Doski FSM (1984). Studies on the origin and synthesis of acid esterase ectoenzyme from human monocytes. Ph. D. Thesis. *Wisconsin-Madison University,* Wisconsin, USA.

Al-Obaidi HA (2006). Microvasculature of the Rat Cerebellum. M.Sc. Thesis. *Al-Nahrain University*.

Al-Salihi AR (1986). Histoenzymatic studies in Duchenne muscular dystrophy. M.Sc. thesis. *University of Baghdad*. Baghdad Iraq.

Al-Salihi AR (2002). Quantitative assay of alpha naphthyl acetate esterases – histochemical characterization. *Iraqi J. Med. Sci*. 1: 398-402.

De Brauwer EIGB, Drent M, Mudler PGH, Bruggeman CA, Wagenaar SS, Jacobs JA (2000). Differential Cell Analysis of Cytocentrifuged Bronchoalveolar Fluid Samples Affected by the Area Counted. *Analytical quantitative Cytology and Histology.* 22: 143-149.

Dethloff LA, Gladen BC, Gilmore LB, Hook GE R (1987). Quantization of cellular and extracellular constituents of the pulmonary lining in rats by using bronchoalveolar lavage. *Am. Rev. Respir. Dis*. 136: 899-907.

Fleury J , EscudierE, Pochelle M-J, Carre C, Bernaudin JF. (1985). Cell population obtained by bronchoalveolar lavage in Pneumocystis carinii pneumonitis. *Acta Cytol.* 29:721–728.

Formigli L, Manneschi LI, Nediani C, Marcelli E, Fratini G, Orlandini SZ, Perna AM (2001). Are Macrophages Involved in Early Myocardial Reperfusion Injury? *Ann Thorac Surg*.71:1596 -602.

Ganz T, Sherman MP, Selsted ME, Lehrcr RI (1985). Newborn rabbit alveolar macrophages are deficient in two microbicidal cationic peptides, MCP-1 and MCP-2. *Am. Rev. Respir. Dis.* 132:901-904.

Henderson AJ (1994). "Bronchoalveolar lavage". *Arch. Dis. Child.* 70: 167–169.

Ibrahim-Granet O, Philippe B, Boleti H, Boisvieux-Ulrich E, Grenet D, Stern M, Latge JP (2003). Phagocytosis and Intracellular Fate of Aspergillus fumigatus Conidia in Alveolar Macrophages. *Infection and Immunity*. 71: 891–903.

Jeffrey MD, Gaston B, Shore SA (1995). Chemical regulation of p1ulmonary airway tone. *Annu. Rev.Physol*.57:151-170.

Jianmin Z, Zhu J, Amy I, Melanie C, Kinane TB, Henry K (2004). *Pneumocystis* Activates Human Alveolar Macrophage NF-kB Signaling through Mannose Receptors. *Infection and Immunity J.* 72: 3147–3160.

Junqueira LC, Carneiro J (2005). Basic Histology, 11th Ed., *McGraw-Hill. New York*. Pp: 357-358.

Khalil N, Whitman C, Zuo L, Danielpour D, Greenbergt A (1993). Regulation of Alveolar Macrophage Transforming Growth Factor-B Secretion by Corticosteroids in Bleomycin-induced Pulmonary Inflammation in the Rat. *J Clin Invest*. 92: 1812-1818.

Lambrecht BN (2006) "Alveolar Macrophage in the Driver's Seat." *Immunity*. 24: 366-368.

Laplante C, Lemaire I (1990). Interactions between alveolar mac-rophage subpopulations modulate their migratory function. *Am J Pathol*. 136:199-206.

Lasbury ME, Durant PJ, Bartlett MS, Smith JW, Lee C-H. (2003). Correlation of Organism Burden and Alveolar Macrophage Counts during Infection with Pneumocystis carinii and Recovery. DOL: *Clin. Diagn. Lab. Immunol*. 10:293-302.

Mansmann RA, King C (1998). How to Perform Bronchoalveolar Lavage in Practice. *Proceedings of the Annual Convention of the AAEP* 44: 186-188.

Oliver C, Lewis PR, Stoward PJ (1991). Esterases. In: Stoward PJ & Pearse AGE (Eds.): Histochemistry - theoretical and applied. Vol. III: Enzyme histochemistry. *4th Ed. Churchill Livingstone*. UK. Pp. 219-239.

Oliver CT, Keefe RG, Sugawara I, Yamada H, Orme I M (2003). SWR Mice Are Highly Susceptible to Pulmonary Infection with Mycobacterium tuberculosis. *Infection and Immunity J*. 71: 5266–5272.

Paul GM, Djano J, Wealthall R, Griffin BJ (2002). Characterization of the Macrophages Associated with the Tunica Vasculosa Lentis of the Rat Eye. *Investigative Ophthalmology & Visual Science*. 43: 2076-2082.

Pugh CW, Gordon MG, Steer HW (1983). Characterization of non-lymphoid cells derived from rat peripheral lymph. *Exp. Med. J.* 157: 1758-1779.

Rao Y, Wong K, Ward M, Jurgensen C, Wu JY (2002). Neuronal migration and molecular conservation with leukocyte Chemotaxis. *Genes & Development* 16:2973–2984.

Rehn B, Bruch J, Zou T, Hobusch G (1992). Recovery of Rat Alveolar Macrophages by Bronchoalveolar Lavage under Normal and Activated Conditions. *Environmental Health Perspectives*. 97:11-16.

Riott I, Brostoff J, Male D (1998). Immunology. 5th ed. *Mosby Company. London*. Pp: 18-30.

Tetuo M, Yoshiko Y, Yokoyama M, Okayasu I (1997). Pulmonary alveolar proteinosis: diagnosis using routinely processed smears of bronchoalveolar lavage fluid. *J. Clin. Patho*. 50: 981-984.

Thompson AB, Teschler h, Wang YM, Konietzko N, Costabel U (1996). Preparation of bronchoalveolar lavage fluid with microscope slide smears. *Eur Respir J*. 9: 603–608.

Wisniowski PE, Spech RP, Wu M, Doyle NA, Pasula R, Martin WJ. (2000) Vitronectin Protects Alveolar Macrophages from Silica Toxicity. *Am J Res Critical Care Medicine*. 162: 733-739.

Zunic SS, SEkulic S, Djordjevic GV, Vukcevic M, Vukcevic PM, Zunic SS, Mandaric D, Obrsdovic VB (1997). Correlation analysis of alveolar macrophage cytochemical parameters in smoking and pulmonoryoncology. *Int J Biol Markers*. 12:79-82.

Ultrastructure of Pancreatic Endocrine Cells of the Single Hump Camel (*Camelus dromedarius*)

Manal Khalid Bsoul[1], Janti |Salahuddin Qar[2], Imad Matloub Al-Ani[2]* and Mohammad Amin Al-Adhami[2]

[1]*Department of Biological Sciences, Faculty of Science, Yarmouk University, Jordan.*

[2] *Department of Basic Medical Sciences, Kulliyyah of Medicine, International Islamic University Malaysia, P.O. Box 141, 25710, Kuantan, Malaysia .*

**Corresponding author: Tel. +60179776014. E-Mail: imad_alani@yahoo.com*

ABSTRACT

The present study was undertaken to provide an ultrastructural identification of the different cells in the islets of the camel pancreas. Tissue samples were obtained from ten healthy, adult camels and processed for electron microscopy. The islets are composed of abundant, centrally located beta; β-cells, alpha; α-cells are present at the very periphery of the islets, while delta; δ-cells are distributed among both β- and α-cells.

These cells were easily distinguished on the basis of the morphology of secretory granules. The granules of the β-cells varied greatly in shape and size and both "dense and pale" granules could be identified. The α-cells have a homogeneous rounded core of moderate to high electron density granules. The δ-cells contain large spherical to irregular shaped granules of variable electron density.

Our findings of the single-humped camel pancreas make additional contribution to those found in other mammalian species.

Keywords: camel, pancreatic islets, beta -cells, alpha-cells, delta-cells, ultrastructure.

INTRODUCTION

The small, pancreatic clusters of endocrine cells were first described by Paul Langerhans in 1869, after whom they were named as "Islets of Langerhans". Since then, many morphological studies have been carried out using histological., histochemical and ultrastructural techniques in human (DeConinck *et al*., 1972; Kim *et al*., 2009) and in a variety of animal species including monkey (Winborn, 1963), cat (Sato *et al*.,1966), rabbit (Williamson *et al*.,1967), rat, dogs and Guinea pig (Watari, 1973), mice (Pictet *et al*.,1967; Al-Ani, 1978), gerbil (Al-Ani, 1987a) and hedgehog (Al-Ani and Al-Mukhtar 1992). The endocrine pancreas has also been studied in-non mammalian species such as chicken (Mikami and Ono, 1962), salamander (Epple, 1966), duck (McClish and Eglitis 1969), teleost fish (Klein and Van Noorden 1980), frog (Etayo *et al*., 2000), and Bowfin fish (Youson *et al*., 2001).

There are three major cell types in the islets of Langerhans: α-cell responsible for the production of glucagon, β-cell for production of insulin, and δ-cell for production of somatostatin; a classification based on the pioneer works of Lacy (1957) and Caramia *et al*., (1965). In addition, other cell types (C, E, F, V and X or PP) responsible for the production of pancreatic polypeptides were rarely observed in a few species such as dog, Guinea pig, rabbit (Volk and wellmen 1977) and mice (Al-Ani 1978).

The single hump camels are domesticated animals, native to the dry desert areas, living in the horn of Africa, the Sahel, Morocco, Middle East and south Asia. They provide people with milk, food and transportation. They are able to withstand changes in body temperature and water consumption. To the best of our knowledge, only two light microscopic studies have investigated the structure of the camel's islets of Langerhans (Khatim *et al*.,1985, Al-Ani 1987b). Therefore, the aim of this investigation is to study the ultrastructural features of the pancreatic islet cells of the camel.

MATERIALS AND METHODS

Small pieces from different parts of the pancreas were collected from ten healthy, adult camels of both sexes at Al-Ramatha slaughter house (Jordan). They were fixed in Bouin's fluid and routinely processed for light microscopy. For electron microscopy, thin slices of pancreatic tissue were fixed in 2.5% glutaraldehyde in 0.1M sodium cacodylate buffer (pH 7.4) for two hours and postfixed for one hour in 1% OsO_4 in the same buffer. They were then dehydrated in acetone and embedded in Spurr's resin. Thick sections (1 μm) were stained with tulidine blue and studied by light microscopy for localization of the pancreatic islets. Thin sections (60-100nm) were cut by LKB ultratome, collected on copper mesh grids, stained with 5 % uranyl acetate and lead citrate. They were examined under Zeiss EM 10 CR.

RESULTS AND DISCUSSION

The present ultrastructural study on the pancreatic endocrine elements has revealed the presence of three well-defined cell types in the islets of Langerhans of the camel. Beta "β" cells, characterized by many, fine, membrane bound granules distributed throughout the cytoplasm. As in islets of many other vertebrates, the most abundant cell is the β-cell; the morphological feature of β-cells in the camel is well correlated with those described in human (Pelletier 1977) and other mammalian species (Hayden *et al*., 2007; Pribac *et al*., 2008; Kocamis *et al*., 2009). They constitute the majority of the islet cells and are mainly located the central area of the pancreatic islets; this is in conformity with previous light microscopic observation of the camel pancreatic islets (Al-Ani, 1987b), however some β-cells are found at the peripheral parts of the islets, this observation is consistent with those reported by Khatim *et al*. (1985) on the camel and Yi *et al*. (2004) on the house musk shrew.

These cells are uniform in appearance with rounded to oval heterochromatic nuclei, their granules vary in shape and size (Figs. 1-4); most of them are spherical or ellipsoid. Some granules are in contact with the plasma membrane (Fig. 4). These contacts might represent the emiocytotic figures originally described by Lacy (1961). They could represent the site of ions and metabolites exchange (Berger *et al*., 1975). The fusion of the granular sac with the plasma membrane is not often observed because the point of opening of secretory granules at the plasma membrane tends to coincide with the plane of the thin section (Orci *et al*., 1973).

The contents of these granules vary extremely in their electron densities and the extent to which they fill the granule and therefore two types of granules "dense and pale" could be identified (Fig. 2). The dense granules have granular contents possessing a central core of electron-dense material with relatively large space between the granule content and its membrane, while the less dense "pale" granules are somewhat larger and occupied a relatively larger volume of their enclosing sacs than the smaller dense granules. The degree to which the granule matrix was separated from its limiting membrane by an electron-opaque region was highly variable in both types of granules. The presence of dense and pale granules in β-cells of the present study; is in conformity with observation on mouse (Al-Ani, 1978), human (Pelletier, 1977), rats (Attia, 2009). Beta cells observed here in the camel corresponds to β1-cells described in some other animals (Lacy, 1961; Thliveris, 1975). The other subtype of β-cells (β2) observed in certain species (Al-Ani, 1978) was not observed in the camel pancreatic islets.

Empty granules were also observed (Figs. 2, 4) the presence of secretory granules with varying electron density and granules lacking core material might suggest that these granules possibly release their contents via intra-granular dissolution of secretory material (β-granulolysis) and its passage into the cell cytoplasm (Al-Ani, 1978; Orci 1985). The mitochondria were either rod or ovoid in shape containing dense matrix with parallel cristae (Figs. 1, 4). Beta cells showed well developed granular endoplasmic reticulum (GER) and Golgi complex (Fig.4).

Junctional complexes (desmosomes and tight junction) were found between some β-cells (Fig. 5); desmosomes were also observed between β-cells of the bovine pancreatic islets (Bonner-Weir and Like 1980). These structures associated with the cytoskeleton provide mechanical stability and are important prerequisites for the acquisition and maintenance of tissue homeostasis (Holthofer *et al*., 2007).

The present study demonstrated the presence of α-cells in the peripheral area of the camel pancreatic islets, they were less numerous and almost polyhedral in shape and their heterochromatic nuclei were spherical to oval with smooth contour (Figs. 3, 6). Their secretory granules showed a homogeneous rounded core of moderate to high electron density and a narrow, lucent halo or well-fitting limiting membrane. The Golgi apparatus consisted of small irregular lamellae and vesicles. The RER consisted of narrow tubules dispersed throughout the cytoplasm and ribosomes were present, both attached to the tubules and free in the cytoplasm, the mitochondria were prominent, and ovoid shaped. The nucleus (Fig. 6) was elongated oval with dispersed heterochromatin. Glucagon has been demonstrated immunocytochemically in many species, such as teleosts (Al-Mahrouki and Youson, 1999), human (Li *et al*., 2002), rabbits (Abdel-Rahman *et al*., 2007) and albino Wistar rats (Kocamis *et al*., 2009).

Delta cells (δ-cells) are generally polygonal or elongated in shape located at the peripheral part of the islet as well as between β-cells, and some time extend within the exocrine tissue. They contain the largest secretory granules among the pancreatic endocrine cells. δ-cells granules were of variable electron density, spherical to irregular in shape, abundant and tightly enclosed by a smooth limiting membrane leaving no halo around the granule core. Lipid droplets were sometimes observed in the cytoplasm and Golgi apparatus was not prominent. The endoplasmic reticulum was dispersed throughout the cytoplasm. Mitochondria were roughly spherical with well developed cristae. The nuclei were irregular in shape with heterochromatin. Delta cells scattered within the exocrine tissue normally exhibited long cytoplasmic processes (Figs. 7, 8). Delta (δ) cells have also been observed in pancreatic islets of the camel. Delta-cells have been identified in the endocrine pancreas of many species including rats (Elayat *et al*., 1995), cats (Legg 1967), pigeons (Kobayashi and Fujita, 1969), Spangue-Dawley rats (Oldsmith *et al*., 1975) and albino Wistar rats (Kocamis *et al*., 2009). Early work has suggested that the δ-cells might be a precursor of a late secretory stage of either α- or β-cells (Creutzfeldt *et al*., 1976). Later imunohistochemical studies demonstrated the presence of somatostatin in the δ-cells of human (Orci *et al*., 1976) and different animal species (Al-Mahrouki and Youson, 1999; Li *et al*., 2002; Oldsmith *et al*., 1975).

It is well known that weather has no direct effect on diabetes control but can affect it indirectly; blood sugar doesn't go up or down in response to hot or cold outdoor temperatures. However heat is a type of stress. Stressors can affect every organ system in the body (Pampori *et al*., 2010). Itoh *et al*., (1998) observed a lower plasma insulin level after glucose and butyrate administrations during hot seasons compared with the thermoneutral environment.

In the desert there is no guarantee in finding food, resulting in intermittent fasting or/ and famine. Long term effects of spaced food intake result in hyperphagia during the repletion periods and a stimulation of lipogenesis and enzyme activities by liver and adipose tissue. These modifications allow the organism to store nutrients rapidly during refeeding after a period of restriction and increase of sensitivity of the β-cell to glucose and a rapid glucose disposal for a minimal insulin secretion (Simon and Rosselin, 1979).

Further immunohistochemical and morphmetric studies on the glucagon-, insulin-, and somatostatin-immunoreactive cells in the pancreatic islets of the camel during seasonal variation are needed.

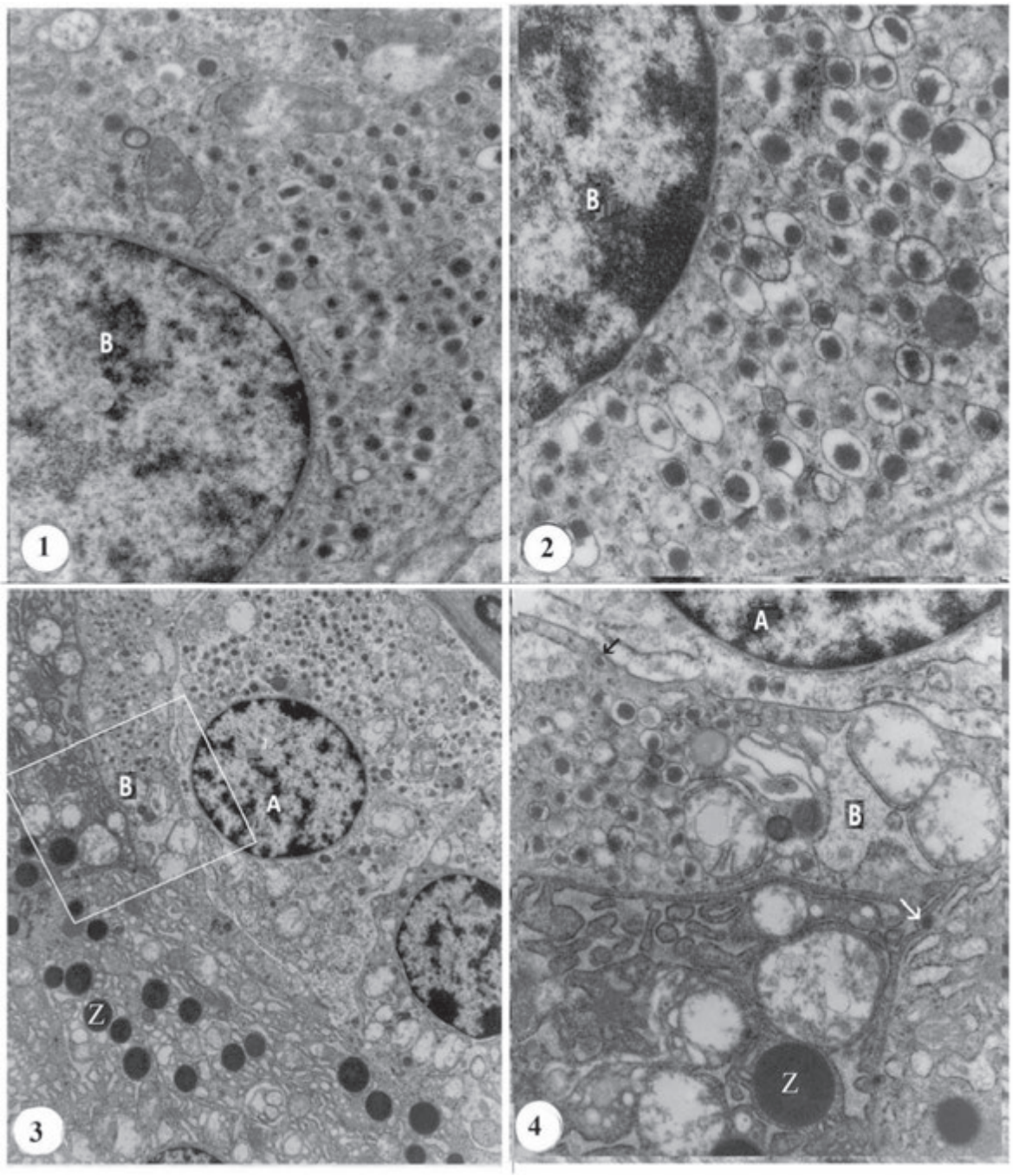

Fig. 1-4. Electron micrographs of camel pancreatic islets.
Fig. 1 & 2 showing β-cells "B" with slightly oval nuclei, the cytoplasm contains numerous secretory granules of different electron density, other secretory granules show the characteristic halo; the core of the granules is polygonal in shape (X : 25,000, X: 40,000, respectively) . Fig. 3 is a peripheral part of the islet near the exocrine pancreas "Z" showing α-cell "A" with extension of β-cells "B" (X: 15,625). Fig. 4 is an enlargement of figure 3 dilated GER, mitochondria and lysosomes and granules near the plasma membranes (exocytosis)"arrows" (X: 25,000).

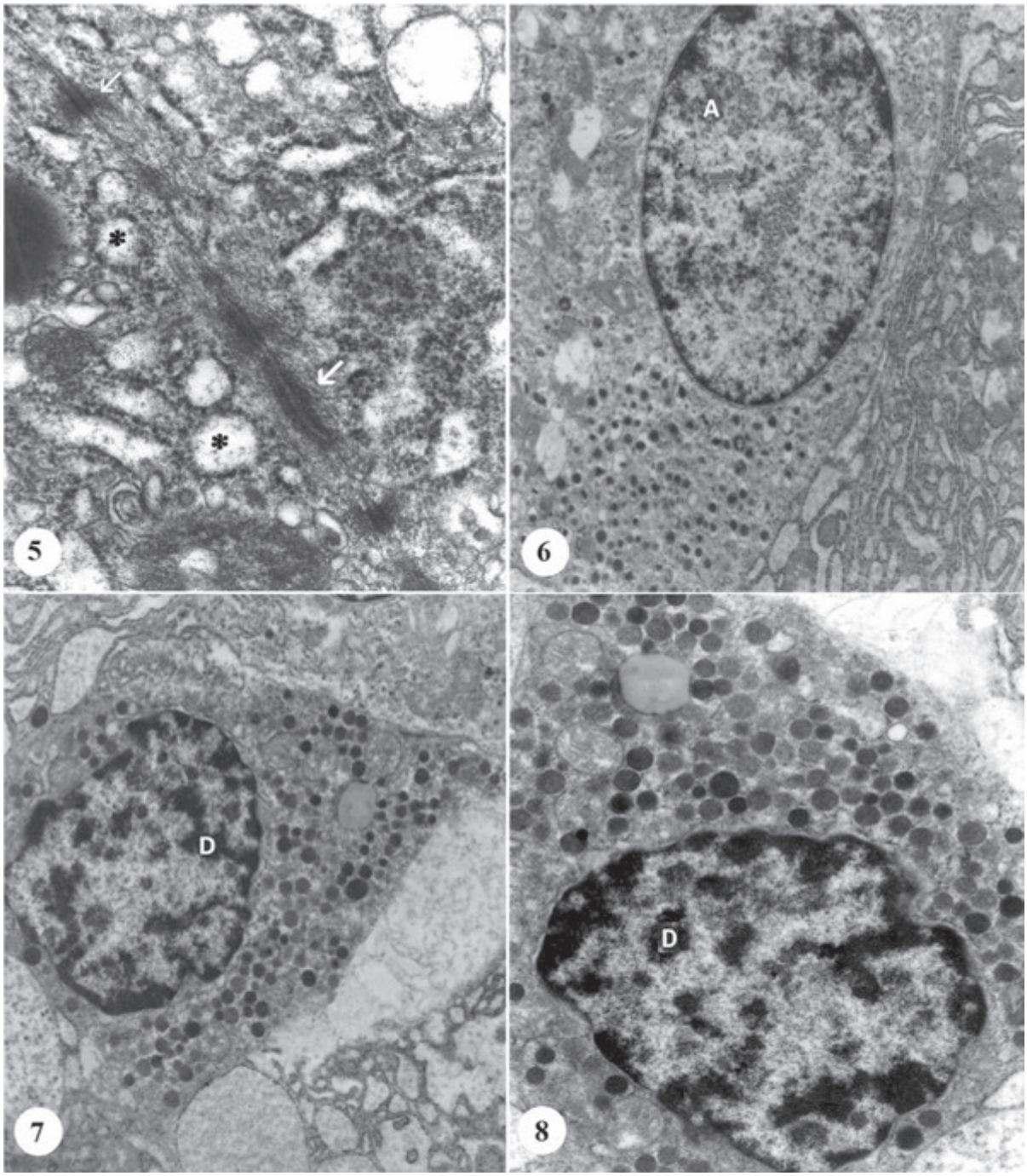

Fig. 5-8. Electron micrographs of camel pancreatic islets. Figure 5. A junctional complex (arrows) between two β-adjacent cells. Rosettes: RER. X: 50,000. Figure 6. An α-cell "A" with oval nucleus and moderate to high electron density granules. X: 10,000. Figures 7, 8. Delta-cell "D" showing large and tightly packed secretory granules, irregular nuclei, lipid droplets, and mitochondrion. X: 10,000, X: 15,625, respectively.

REFERENCES

Abdel-Rahman AH, Hassan HA, Kasem MA, Osman HE, Abdel-Hamid HS, El- Basil M, Mashahit MA (2007). Effects of aging on pancreatic islet cell function: An experimental immunohistochemical and ultrastructural study. *Egyptian Journal of Hospital Medicine*, 29: 591– 603.

Al-Ani IM. (1978). Histochemical and ultrastructural studies on the islets of Langerhans of lean and obese hyperglycemic mice with age. M. Phil Thesis. The University of Aston in Birmingham. Birmingham, England.

Al-Ani IM. (1987a). The ultrastructure of pancreatic islets of the monogonial gerbil *Meriones unguiculatis*. *J. Biol. Sci. Res*, 18: 141-153.

Al-Ani IM. (1987b) Light Microscopy of the camel's (*Camelus dromedarius*) islets of Langerhans. *J. Biol. Scientific Res*, 18:75-80.

Al-Ani IM and Al-Mukhtar KA. (1992). Histological structure of the endocrine pancreas of the Hedgehog "*Hemiechinus auritus' Iraqi J. Biol. Sci*, 11: 25-36.

Al-Mahrouki AA, Youson JH(1999). Ultrastructure and immunocytochemistry of the islet organ of Osteoglossomorpha (Teleostei). *General and Comparative Endocrinology*, 116: 409–421.

Attia AA (2009). Histological and electron microscopic studies of the effect of β-Caroene on the pancreas of Streptozotocin (STZ) induced diabetic rats. *Pakistan J.Biol.Sci*, 12: 301-304.

Berger W, Dahl G Meissner HP (1975). Structural and functional alteration in fused membranes of secretory granules during exocytosis in pancreatic islet cells of the mouse. *Cytobiologi*e, 12: 119-139.

Bonner-Weir S, Like AA (1980). A dual population of islet of Langerhans in Bovine pancreas. *Cell Tissue Res*, 206: 157-170.

Caramia F, Munger BL, Lacy PE (1965). The ultrastructural basis for the identification of cell types in the pancreatic islets I. Guinea pig. *Cell and Tissue Research*, 67: 533-546.

Creutzfeldt W, Creutzfeldt C, Frerichs H, Track N, Arnold R, (1976). Histochemistry, ultrastructure and hormone content of human insulinomas. *Horm Metab Res*, 6:7-18.

DeConinck JF, Van Assch FA, Potvliege PR, Gepts W (1972). The ultrastructure of human pancreatic islets. The islets of neonates. *Diabetologia*, 8:326-333.

Elayat AA, El-naggar MM, Tahir M (1995) An immunocytochemical and Morphmetric study of the rat pancreatic islets. *J. Anat*, 186: 629–637.

Epple, A. (1966). Islet cytology in urodele amphibians. *General and Comparative Endocrinology*, 7: 207-214.

Etayo JC, Montuenga LM, Sesma P, Dı´az de Rada O, Rovira J, Villaro AC (2000). Characterization of pancreatic endocrine cells of the European common frog Rana temporaria. *General and Comparative Endocrinology*, 117, 366–380.

Hayden MR, Karuparthi PR, Habibi J, Wasekar C, Lastra G, Manrique C, Stas C, Sowers JR (2007). Ultrastructural Islet Study of Early Fibrosis in the Ren2 Rat Model of Hypertension. Emerging Role of the Islet Pancreatic Pericyte-Stellate Cell. JOP. *J Pancreas*, 8:725-738.

Holthofer B, Windoffer R, Troynovsky R, Leube RE (2007). Structure and function of Desmosomes. *International Review of Cytology*, 264:65-163.

Itoh F, Obara Y, Rose MT, Fuse H (1998). Heat influences on plasma insulin and glucagon in response to secretogogues in non-lactating dairy cows. *Domestic Animal Endocrinology*, 15:499-510.

Khatim MS, Gumaa KA, Petersson B, Lundqvist G, Grimelius L, Hellerström C. (1985).The structure and hormone content of the endocrine pancreas of the one-humped camel (Camelus dromedarius). *Anat Anz*, 159:181-186.

Kim A, Miller K, Jo J, Kilimnik G, Wojcik P, Hara M. (2009) Islet architecture: a comparative study. *Islets*, 1: 129-136.

Klein C, and Van Noorden S. (1980). Pancreatic polypeptide (PP)- and glucagon cells in the pancreatic islet of Xiphophorus helleri H. (Teleostei). Correlative immunohistochemistry and electron microscopy. *Cell Tissue Res*, 205: 187-198.

Kobayashi S, Fujita T (1969). Fine structure of mammalian and avian pancreatic islets. *Z Zellforsch*, 100:340–363.

Kocamis H, Sari EK, Nazli M, Gulmez N, Aslan S, Deprem T (2009). Immunohistochemical Distribution of Insulin-, Glucagon-, and Somatostatin-Containing Cells in the Pancreas of the

Rat. Kafkas Univ Vet Fak Derg, 15: 611-614.

Lacy PE. (1957). Electron microscopic identification of different cell types in the Islets of Langerhans of Guinea pig, rat, rabbit and dog. *Anat. Rec*, 128: 255-267.

Lacy PE. (1961). Electron microscopy of β-cell of pancreas. *Am. J. Medicine*, 31: 851-859.

Legg PG (1967). The fine structure and innervations of the beta and delta cells in the islets of Langerhans of the cat. *Z. Zellforsch*, 80: 307-321.

Li G, Ye L, Yang W, lou J. (2002). Impact of isl*et al*pha cell loss on insulin secretion. *Zhonghua Yi Xue Za Zhi*, 82:1427-1431.

McClish RD and Eglitis JA. (1969). Distribution of the A and B cells and of the islets (Langerhans) in the duck pancreas. *Ohio Journal of Science*, 69: 285-293.

Mikami, S. and Ono, K. (1962). Glucagon deficiency induced by extirpation of alpha islets of the fowl pancreas. *Endocrinology*, 71: 464-473.

Oldsmith PC, Rose JC, Arimuar A, Ganong WF (1975). Ultrastructural localization of somatostatin in pancreatic islets of the rats. Endocrinology, 97:1061-1064. Orci L. (1985) The insulin factory: a tour of the plant surroundings and a visit to the assembly line. The Minkowski lecture 1973 revisited. *Diabetologia*, 28:528–546.

Orci L, Amherdt M, Malaisse-Lagae F, Rouiller C, Renold AE (1973) Insulin release by emiocytosis. *Science*, 179: 82-84.

Orci L, Baetens D, Rufener C, Amherdt M, Ravazzola M, Studert P, Malaisse-Lagae F, Ungert RH. (1976). Hypertrophy and hyperplasia of somatostatin-containing D-cells in diabetes. Proc nat Acad Sci USA 73: 1338-1342.

Pampori ZA, Huozh R, Shah KA, Andrabi SA, Amin T (2010) Stress Versus Reproduction in Animals. Online Vet J, 5: Article 61.

Pelletier G (1977) Identification of Four Cell Types in the Human Endocrine Pancreas By Immunoelectron Microscopy. *Diabetes*, 26: 749-756.

Pictet R, Orci A, Gonet AE, Rouiller C, REnold AE. (1967). Ultrastructural studies of the hyperplasic islets of Langerhans of spiny mice (*Acomys cahirinus*) before and during the development of hyperglycemia. *Diabetologia*, 3:188-211.

Pribac G, Craciun C, Szoke-Nagy T, Simeoni I, Lang C, Rosioru C, Czapar M, Mathe E, Mos L, Ardelean A. (2008). Comparative ultrastructural study of pancreatic beta cells from diabetic rats treated with fenugreek seed flour or ganoderma flour. Annals of RSCB, XVI: 62-80.

Sato T, Herman L, Fitzgerald PJ. (1966). The comparative ultrastructure of the pancreatic islets of Langerhans. *General Comparative Endocrinology*, 7: 132-136.

Simon J, Rosselin G (1979). Effect of Intermittent Feeding on Glucose-Insulin relationship in the Chicken. *J. Nutr*, 109: 631-641.

Thliveris JA. (1975). Fine structure of foetal rat pancreatic alpha and beta cells. Virchous *Arch.* B-cell Path, 19: 157-165.

Volk BW and wellmen KF. (1977). The Diabetic pancreas. Baillière Tindall, London.

Watari, N. (1973). Castro-Entero-Pancreatic Endocrine System. A Cell- Biological Approach, ed. by FUJITA, T., Igaku Shoin Ltd., pp. 71-89.

Winborn, W. B. (1963). Light and electron microscopy of the islets of Langerhans of the Saimiri monkey pancreas. *Anat. Rec*, 147: 65-94.

Williamson, Lacy PE, Taylor KW. (1967). Electron Microscopy of Islets of Langerhans in rabbit pancreas Slices Incubated in vitro. *Biochem. J*, 102: 928-929.

Yi, Shuang-Qin, Keiichi Akita, Tetsuo Ohta, Takashi Shimokawa, Ai Tanaka, Fei Ru, Toshio Nakatani, Genzoh Isomura, Shigenori Tanaka. 2004. Cellular localization of endocrine cells in the adult pancreas of the house muskshrew, Suncus murinus: a comparative immunocytochemical study. *General and Comparative Endocrinology*, 136: 162–170.

Youson JH, Al-Mahrouki AA, Naumovski D, Conlon JM. (2001). The endocrine cells in the gastroenteropancreatic system of the bowfin, Amia calva L.: An immunohistochemical., ultrastructural., and immunocytochemical analysis. *Journal of Morphology*, 250: 208–224.

Evaluation the Histological and Ultrastructural Effects of Diode Laser Irradiations on the Hard Palate of Domestic Rabbits

Fatin Latif Al-Ogaily[1], Alaa A. Sawad[2]* and Karim A. Al-Jashmy[3]
[1]*Department of Basic Science, College of Dentistry, University of Basra, Iraq*
[2]*Department of Anatomy, College of Veterinary Medicine, University of Basra, Iraq*
[3]*Pathology Unite, Faculty of Medicine, SEGi University, Malaysia*
**Correspondence email: alaasawad65@yahoo.com*

ABSTRACT

The present study was conducted in the college of Veterinary Medicine- University of Basrah to demonstrate the histological and ultrastructural changes that occurred by using Diode laser (490 nm) and to trace their effects on the lining tissue of the hard palate in domestic rabbits. The objective of this study was to evaluation the histological and ultrastructural effects of Diode Laser irradiations on the hard palate on domestic rabbits. These animals divided into two equal groups name diode laser group (DLG), the animals were exposed to wavelength 490nm, and the control group (CG). All animals in DLG exposed to 490 nm wavelength on distance 10 cm about the target tissues of the oral cavity. The results of this study showed the CG hard palates mucosa consisted of heavily keratinized stratified sqaumous epithelium that forms deep epithelial papillae. The DLG on five minutes irradiation for 7 days showed mild detachment of the epithelial surface associated with vacuolar degeneration, while at 10 minutes irradiation for 14 days showed keratinized layer separated from the epithelial layer, with sever hemorrhage in connective tissue. At 30 minutes irradiations for 21 days showed sever detachment of epithelial layer associated with degenerative regions and necrosis were seen. Ultrastructural changes after 30 minutes irradiation of the hard palate mucosa showed partially destroyed of the basal lamina structures. The granulosum epithelial cells observed in elongated shape with altered nuclei and mitochondria. A number of vacuoles and nuclear outline were irregular while parts of the nuclear membrane showed an increased of tonofilaments in epithelial cells. Fibroblast cells with irregular nuclei and large lipid droplet dispersed in lamina properia were also observed.

Keywords: Histology, Ultrastructural, Diode Laser, Hard Palate, Rabbits

INTRODUCTION

The word LASER is an acronym for "Light Amplification by Stimulated Emission of Radiation". Laser is a device that transforms light of various frequencies into a chromatic radiation in the visible, infrared and ultraviolet regions with all waves in a phase capable of mobilizing immense heat and power when focused at a close range (Donald, 2000). The radiation of laser possessed only a single wavelength a propagated almost parallel, along a certain axis. The photons that make up the energy beam are emitted as coherent (in phase), unidirectional, monochromatic light, which is culminated into an intensely focused beam. As laser beams are in the infrared range, they are not visible; thus a quartz fiber channeling a red light is incorporated into the device to act as an aiming beam (Cobb, 2006).

The use of laser in medicine presents a special interest due to the spectacular progresses recorded in the treatment of various conditions. Lasers, like all light not only behave as a particle and wave but also possess several unique characteristics. Lasers are monochromatic and contain light of a very narrow bandwidth. The most common effects of laser on oral mucosa were shown in several studies. The typical thermal damage in laser treated tissues has shown when studying the tissues of the oral cavity by Fisher *et al*. (1983) and Verschueren (1976) while the effects of CO2 laser on excisional tongue tissue include: carbonization in the layer at the level of the excisional margin and vacuolar degeneration and elongation of nuclei in the deeper layers (Mausberg *et al*., 1993).

The effects of laser on the oral cavity and oral mucosa have been shown by several experimental ultrastructural studies on the oral tissues. Pervious studied on the the skin (Ben Bassat and Kaplan

1976) and the skeletal muscles (Viehberger *et al*.,1979) reported that ultrastructural effect of the CO_2 laser and regarded them as signs of thermal damage. Visuri *et al*., (1996) showed by scanning electron microscope analysis that the Er: YAG laser created open dentin tubules that allowed for the development of resin. Also, ultrastructural studies have shown effects on the mucosal fungiform papillae of the tongue in rats after irradiation. Several studies revealed degenerative nuclei as well as most of the cell organelles in the basal layer of the fungiform papillae (Obtinata *et al*., 1997; Just *et al*., 2005). Few reports that documented of the rules of the laser in the hard palate experimentally, hence the objective of this study was to evaluation the histological and ultrastructural effects of Diode Laser irradiations on the hard palate on domestic rabbits

MATERIALS AND METHODS

In this study 24 domestic rabbits were randomly selected. At 5 months old and weighting 2.5-3.0 kg, the animals were housed in clear wood cages and fed with vegetables and tap water under the same of the laboratory environment. These animals were divided into two equal groups, name by diode laser group (DLG), where the animals were exposed to wavelength 490nm, and the control group (CG).

All animals in DLG were anesthetized with intramuscular administration (IM) of 10mg\ kg body weight xylazine hydrochloride and 0.5 mg /kg body weight ketamine hydrochloride, and fixed on a coach that prevented them from the motion during the exposure period. After anesthetizing, the animal oral cavity was opened using mouth gag, then animals were exposed to 490 nm wavelength at a distance of 10 cm from the target tissues of the oral cavity. Laser rays were given once daily at 5, 10 and 30 minutes for 7, 14 and 21days respectively.

At the end of exposure time, all animals were ssacrificed by air bubbles in the heart, and the specimens were collected from the hard palate. Specimens of whole target oral tissues were fixed immediately in 10% formalin. Fixed tissues were washed in current water, dehydrated in a graded series of alcohol, cleared in xylene and embedded in paraffin wax. Serial sections of five micrometers thick were made. Mounted on slides, the sections were stained with haematoxylin and eosin (Luna 1968). The histological sections were studied under the light microscope on 10x, 40x, 100x and the photographic pictures were taken from the sections of tissues by using a light-microscope (Leica DM 500 from Germany).

For electron microscope techniques, the specimens were taken from the hard palates after being irradiated with 30 minutes of diode laser for 21 days only. The specimens were fixed in 5% glutaraldehyde in 0.1 M sodium cacodylate buffer (pH 7.3) for 3-4 hours (Karnovsky, 1965). They were washed twice for 10 minutes each in sodium cacodylate buffer and then post fixed in 1% osmium tetroxide in the same buffer for 2 hours. Then the fragments were dehydrated in an increasing series of ethanol alcohol solutions (10%, 30%, 50%, 70% and 100%) for 30 minutes each. After the dehydration process, the fragments were put in a mixture of absolute alcohol and propylene oxide 1:1 for 30 minutes and embedded in Epon resin. The samples were cut into to ultrathin sections (75-nm) by an ultramicrotome, Ultra-Cut with a diamond knife (LKB Broma 2200, Sweden). The ultrathin sections were mounted on 200 and 300 mesh grids and they were counterstained with uranyl acetate and lead citrate for 10 minutes (Reynolds, 1963; Watson, 1958). The sections were then examined and photographed using a transmission electron microscope (JEM-2200 FS\CR, Jeol, Japan).

RESULT

The results of this study showed the CG hard palates mucosa consisted of heavily keratinized stratified sqaumous epithelium that formed deep epithelial papillae, which were arranged in rows. The lamina properia contain thick collagen bundles and relatively a little ground substance and submucosa was absent (Fig. 1). The DLG on five minutes irradiation for 7 days showed mild

detachment of the epithelial surface associated with vacuolar degeneration of the cells were seen inside the epithelial layer of this tissue (Fig. 2), while on 10 minutes irradiation for 14 days suffering from separating of the keratinized layer from the epithelial layer, with sever hemorrhage in connective tissue (Fig. 3). On 30 minutes irradiation for 21 days showed sever detachment of epithelial layer associated with degenerative regions, pyknotic cell nuclei and necrosis (Fig. 4).

Ultrastructural changes after 30 minutes irradiation of the hard palate mucosa with diode laser showed that the basal lamina structures were partially disrupted (Fig. 5). The granulosum epithelial cells could be observed in elongated shape with altered nuclei and alerted mitochondria. The nuclei of affected cells had granulated chromatin. A number of vacuoles were present and the nuclear outlines were irregular while parts of the nuclear membrane were unclear as compared with normal granulosum cells. They were associated with an increased tonofilaments in epithelial cells and active mitochondria. Fibroblast cells with irregular nuclei and large lipid droplets dispersed in lamina propria were seen (Fig. 7).

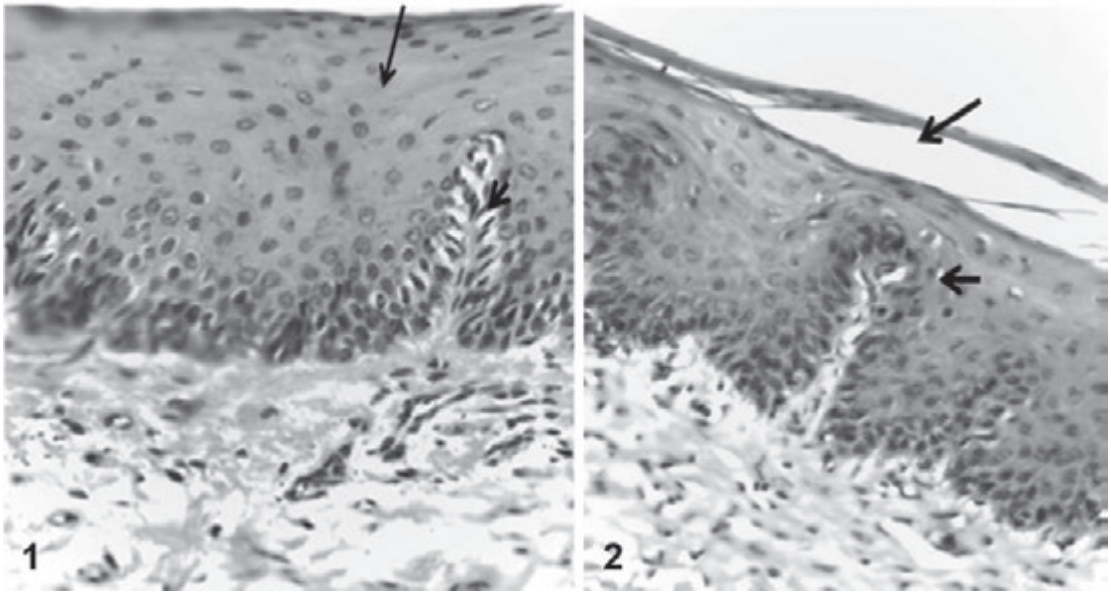

Fig. 1: The hard palate showe keratinized epithelial layer (long arrow), Lamina propria (short arrow) H&E400X.
Fig. 2: The hard palate showed the effect of Diode Laser at 5 minutes Irradiation: mild detachment of the epithelial surface (long arrow) and vacuolar degeneration (short arrow) H&E 400X.

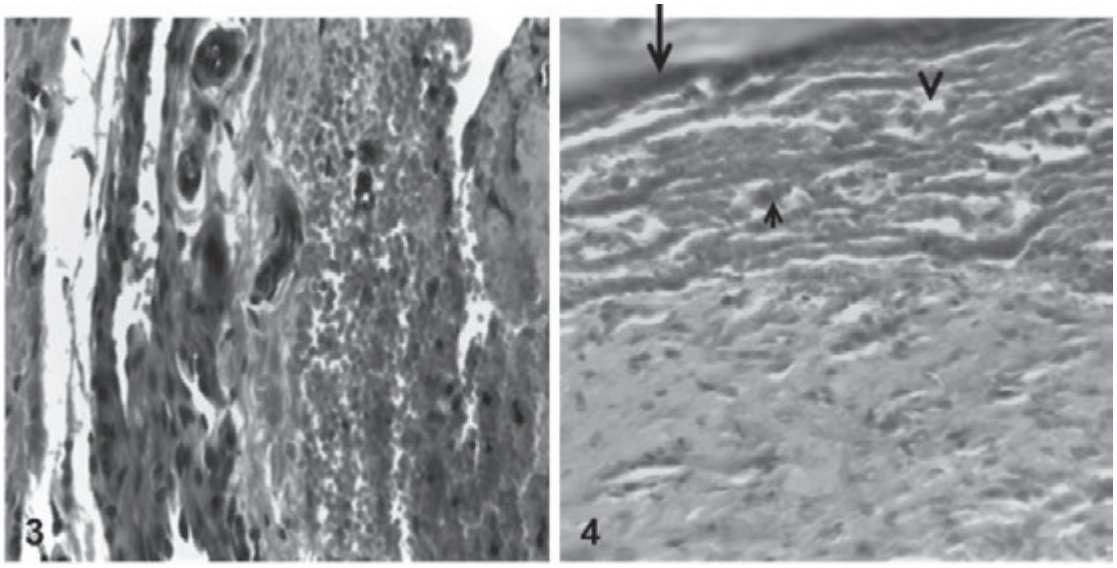

Fig. 3: The hard palate treated with effect of Diode Laser-10 minutes): shows sever hemorrhage H&E 400X.
Fig. 4: The hard palate effected of Diode Laser-30 minutes irradiation): Shows necrosis (arrow head) pyknotic nuclei (short arrow) and severe detachment of epithelial layer (long arrow) H&E 400X

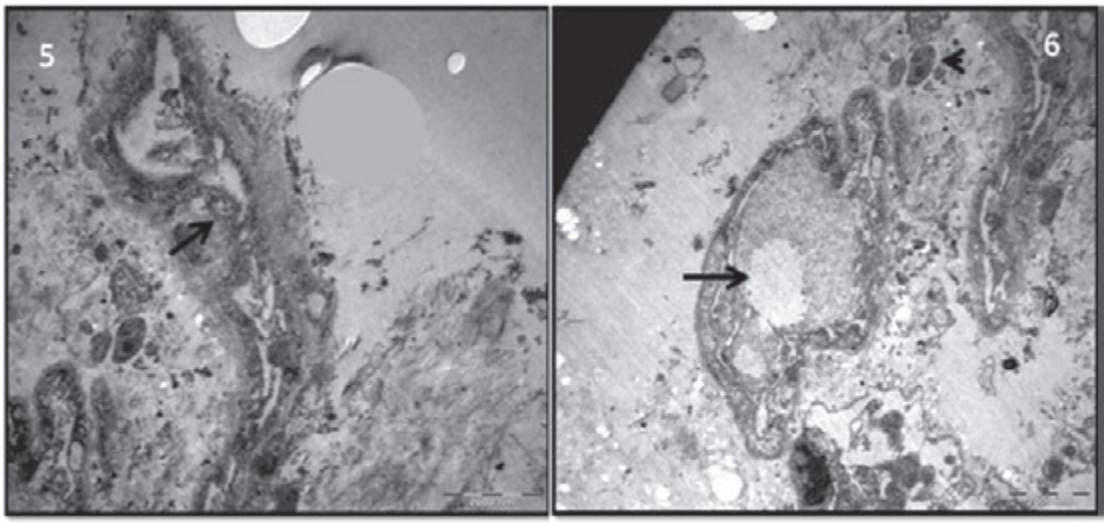

Fig. 5: Transmission electron micrograph of hard palate mucosa after irradiated with Diode Laser at 30-minutes irradiation shows the basal lamina structures are partially disrupted (arrow) 30,000X.
Fig. 6: Transmission electron micrograph of hard palate mucosa after irradiated with Diode Laser at -30 minutes irradiation shows the granulosum cells had vacuolated nuclei (arrow) and alerted mitochondria (arrow head) 30,000X.

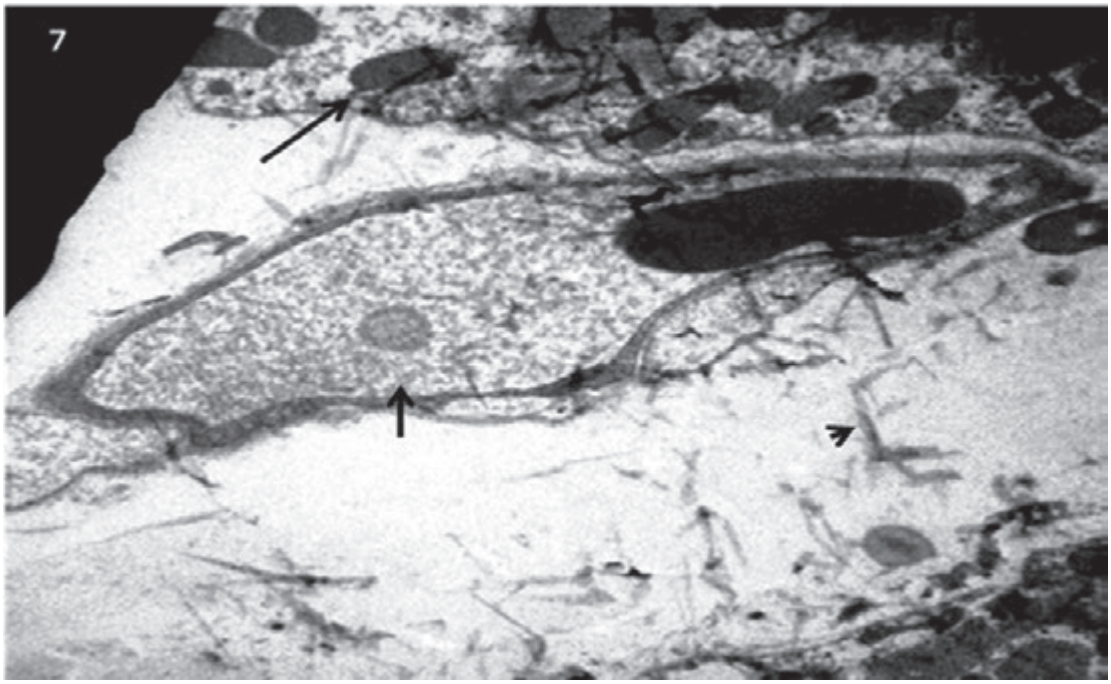

Figure (7): Transmission electron micrograph of hard palate mucosa after irradiated with Diode Laser at-30 minutes irradiation shows fibroblast (short arrow) and active mitochondria (long arrow) and tonofilaments (arrow head) 10,000X.

DISCUSSION

The study was designed to demonstrate the histological changes and levels of damage that might occurred on oral hard palate mucosa after using a diode laser of wavelength 490nm, The biological effects of laser beams on tissues have been thoroughly investigated by Bryant *et al* (1998), Fisher and Frame (1984) and Carew *et al* (1998). The effect of the five minute period includes mild detachment of the epithelial surface of the hard palate and soft palate. This result is

similar to that found by Goharkhay *et al*. (1999). The vacuolation of the cells due to the effect of diode laser on these tissues was shown by Maiorana *et al*., (2002) as a result from the thermal effect of the diode laser beam. In hard palate tissues after a ten minute irradiation, there was a severe hemorrhage. This result disagrees with Goharkhay *et al., (*1999) and Rizoiu *et al*., (1996) who studied the effect of Er,Cr:YSGG and diode laser in an animal model, New Zealand White rabbit, and responded minimal bleeding.

The necrosis indicates the main histological changes of hard palate as a result from the effect of diode laser on this tissue. Pyknotic cell nuclei also was observed after thirty minutes irradiation. The ultrastructural observations showed that several structural alterations were detected in the hard palate mucosa after irradiation with diode laser such as partially destroyed basal lamina structures, granulosum epithelial cells with altered nuclei and mitochondria, as well as large vacuoles in the nuclei of these cells. Multinucleated cell also could be detected, this histopathological finding was detected by Obtinata *et al*., (1997), Just *et al*., (2005), Gomes *et al*., (2002) and Stern *et al*., (1972). The basal epithelial cells showed altered nuclei and mitochondria morphology as well as large spaces in lamina propria and large lipid droplets. Increased intracellular space and lipid droplets were described in previous reports (Martinez *et al*., 2005; Zorzetto *et al*., 2002).

The monochromatic light wavelengths are well ordered and remain synchronized with one another (Tuner and Hode, 2004). This quality described as coherence, means that all of the laser waves are the same shape, that they have the same peaks and valleys (Bradley and Turner, 2007; Coluzzi, 2004). Laser are widely used in the clinics nowadays. An example from present day dentistry serves as an excellent example of light interferences. Popular light emitting diode (LED) curing units are used by dentists and orthodontists all over the world for curing adhesives and composite resins (Vandewalle *et al*., 2005; Kramer *et al*., 2008).

REFRENCES

Ben Bassat, M. and Kaplan, I. (1976). A study of the ultra structural features of the cut margin of skin and mucous membrane specimens excised by carbon dioxide laser. *J. Surg. Res*. 21, 77.

Bradley, P. and Tunér, J. (2007). Laser Phototherapy in Dentistry. In: Proceedings of the 1st International Workshop of Evidence Based Dentistry on Lasers in Dentistry. 1st ed London: *Quintessence Publishing Co. Ltd*: 149-71.

Bryant, G.L., Davidson, J.M., Ossoff, R.H., Garret, C.G. and Reinisch, L. (1998) Histological study of oral mucosa wound healing: comparison of a 6.0-to 6.8 –micrometer pulsed laser and a carbon dioxide laser.*Laryngoscope*.108:13-17

Carew, J.F., Ward, R.F., Labruna, A, Torzilli, P.A. and Schley, W.S.L. (1998). Effect of scalpel, elctrocautery and Co2 and KTP lasers on wound healing in rat tongue. *Laryngoscope*.108:373-390.

Cobb,C.M.(2006).Lasersinperiodontics:areviewoftheliterature.*J.Periodontal.*;77(4):545-64.

Coluzzi, D.J. (2004). Fundamentals of dental laser: science and instruments. *Dent Clin North Am*;48:751-70.

Donald, J.C. (2000). An overview of laser wavelengths used in dentistry. *DCNA*.; 44(4).

Fisher, S.E. and Frame, J.W. (1984).The effects of the carbon dioxide surgical laser on oral tissues. *Br. J. Oral Maxillofacial. Surg.*22, 414–425.

Fisher, S.E., Frame, J.W. and Browne, R.M..(1983). Comparative histological study of wound healing following C02 laser and conventional surgical excision of canine buccal mucosa. *Arch. Oral. Biol*. 28,287-291.

Goharkhay, K., Moritz, A., Wilder-Smith, P., Schoop, U., Kluger, W., Jakolitsch, S. and Sperr, W.(1999). Effects on oral soft tissue produced by a diode laser in vitro. *Lasers Surg Med*. 25(5): 401-406.

Gomes, I., Cagnon, V.H.A. , Carvalho, C.A.F. and DeLuca, I.M.S. (2002). Stereo logy and

ultra structure of the seminal vesicles of C57-BL-6J mice following chronic alcohol ingestion. *Tissue Cell* 34,177-186.

Just, T., Pau, H.W, Bombor, I., Guthoff, R.F., Fietkau,R. and Hummel, T. (2005): Confocal microscopy of the peripheral gustatory system: comparison between healthy subjects and patients suffering from taste disorders during radio chemotherapy. *Laryngoscope*; 115(12):2178-82.

Kramer, N., Lohbauer, U., García-Godoy, F. and Frankenberg, R. (2008). Light curing of resin-based composites in the LED era. *Am J Dent*; 21:135-42.

Luna L, L. G. (1968). Manual of histological staining methods of the force institute of pathology, 3rd (ed) McGraw. *Hill book, New York*: 258.

Maiorana ,C., Salina, S. and Santoro, S. (2002). Treatment of Periimplantitis with Diode Laser: A Clinical Report. *J Oral Laser Applications*, 2: 121- 127.

Martinez, M., Milton F.A., Oliveira, S.A. and Lima, N.F. (2005). Ultrastructural changes on the hard palatine mucosa of Calomys callosus after 120 days of experimental chronic alcoholism. ubmicrosc. *Cytol. Pathol*. 37 (1), 59–65.

Mausberg, R., Visser, H., Aschoff, T., Donath, K. and Kruqer, W. (1993). Histology of laser- and high-frequency electrosurgical incisions in the palate of pig. *J. Craniomaxillofac. Surg.* 21, 130–132.

Obtinata, K., Ohshima, H., Takano, Y. and Ito, J. (1997): Early ultra structural changes in the dorsal mucosa of rat tongue after irradiation, with special reference to the microvasculature. *Radiate Med;* 15(5): 305-15.

Reynolds, S.L. (1963). The use of lead citrate at high PH as an electron-opaque stain in electron microscopy. *J. Cell Biol*.71, 208-212.

Rizoiu, I.M., Eversole, L.R. and Kimmel, A.I. (1996). Effect of an erbium, chromium : yttrium , scandium , gallium , garnet laser on mucocutanous soft tissues. *Oral surg Oral Med pathol Oral Radiol Endod*. 82: 386-95.

Stern, R.H., Vahl, J. and Sognnaes, R.F. (1972). Lased enamel:ultrastructural observation of pulsed carbon dioxide laser effects Dent Res; 51:455-460. study of CO2 and Er:YAG laser effect on oral soft tissues. *Photo med. Laser. Surg*. 22, 185–189.

Tuner, J. and Hode, L.(2004). The Laser Therapy Handbook. 1st ed. *Grangesberg, Sweden: Prima Books* AB;:12-7.

Vandewalle, K.S., Roberts, H.W., Andrus, J.L. and Dunn, W.J (2005). Effect of light dispersion of LED curing lights on resin composite polymerization. *J Esthet Rector Dent*;17:244-55.

Verschueren, R.C. (1976).The C02 Laser in Tumor Surgery. *Amsterdam: Gorcum. Assen.*

Viehberger, G., Fischer, R. and Kyrie, P. (1979). Ultra structure of skeletal muscle after C02 laser. *Res.Exp. Med.* (Berl.) 176,69.

Visuri,S.R., Gilbert, J.L., Wright, D.D., Wigdor, H.A. and Walsh, J.J. Jr.(1996). Shear strength of composite bonded to Er:YAG laser prepared dentin. *J. Dent.Res*.,75:599-605.

Watson, M.L. (1958). Staining of tissue sections for electron microscopy with heavy metals.*J.Biophys.Biochem.Cytol*.4,727-730.

Zorzetto, D.L., Garcia, P.J., Toledo Filho, J.L. and Zorzetto, N.L. (2002). Ultrastructural study of the cheek oral mucosa of rats submitted to experimental chronic alcoholism. Submicrosc. *Cytol. Pathol*. 34 (3), 345–353.

High Voltage Electron Microscopic X-ray Point Quantification of the Ultrastructural Localization of Cellular Lysosomal Enzyme Activity

Akihiro Nohara Olea
Université des Sciences et des Technologies de Hanoi (USTH), Hanoi, VN
**correspondence email: mel_ole@hotmail.com*

ABSTRACT

Lysosomes are membrane-limited cytoplasmic organelle containing large number of hydrolytic enzymes which are responsible for cellular digestion. Hence, they are in abundance in cells undergoing phagocytic activity. Acid phosphatase (AcP) is one of the enzymes present in the organelle which has been characterized as the marker enzyme for lysosome. Likewise, the use of acid phosphatase (AcP) as a marker enzyme for cell death and/or cell undergoing lysis has been established. The present study was undertaken to determine the enzyme activity in the lysosome and possibly relate the result to maturational development of the animals. The study used ddY strain mice ages ranging from 1 day to 10 months old. The Lanthanide-based method for the ultrastructural localization of AcP was employed. The results of the study showed that the fine localization of AcP was observed in the proximal tubule cells, particularly of the second segment of the mouse kidney. The result of AcP activity as manifested by the dense reaction product was observed in the lysosome and appeared homogeneous, while in other organelles it appeared heterogeneous. The main spectral line of cerium at Lα=4.84KeV and Lβ=5.26keV was used in the quantitative determination of the peak-to-background (P/B) ratio. The results showed an increase in AcP activity from day old animal, reaching a peak in one week old and thereafter, activity was observed to decrease consistently until the 10 month-old-animals.

KEYWORDS: Acid Phosphatase (AcP), EM cytochemistry, mouse kidney, maturational development

INTRODUCTION

In 1949 a Belgium scientist, Christian de Duve discovered one of the cellular organelles identified as lysosomes. The organelles are present in the animal cells and contain hydrolytic enzymes, responsible for breaking down cellular wastes and debris. Lysosomes digest worn-out and/or damaged organelles, food particles and even engulf microorganisms like bacteria and viruses. Generally, the organelle fuses with autophagic vacuoles, releasing the enzymes into it and then digests the content. Most often, because of the ability of the organelle to self-digest through the action of the enzyme, it is often referred to as "suicide-bag". The size of the lysosome varies and range from 0.1μm to 1.2μm (Kuehnel, 2003) and because of the presence of acidic enzymes, the interior of the organelle has a pH 4.8. The enzymes are known to be capable of providing phosphate to tissues that are in need of high energy requirement, particularly during development, growth and maturation of the animal (Hurkadli *et al*, 1985; Blum, 1970). Although the hydrolases present in the lysosomes share a common functionality, they could be differentiated according to the structure, catalytic properties and, tissue and sub-cellular distribution (Suter *et al*, 2001).

Acid phosphatase (AcP) is one of the hydrolytic enzymes present in the organelle and it serves as the marker enzyme for lysosomes (Weiss, 1988; Veenhuis, *et al*, 1980). Likewise, the use of the acid phosphatase enzyme activity in the lysosome as a marker enzyme for cells undergoing lysis and cell death has been reported (Bowen and Lewis, 1980).

In the kidney, reports have shown that the AcP enzyme have been localized in the lysosomes throughout the second segment of the proximal tubule cells of the kidney of the mouse (Maunsbach, 1966).

The present study was undertaken to determine the specific ultrastructural localization of acid phosphatase (AcP) enzyme activity in the cellular lysosome of mouse kidney. In addition, the study attempted to determine the level of enzyme activity in the animal cellular lysosome as

measured quantitatively by point X-ray microanalysis. The results of the quantitative analysis were compared among the different ages of the animals and implicate the result to the growth, differentiation and development of the animals.

MATERIALS AND METHODS

A. Experimental Animals and Pre-fixations

The animal used in the study is composed of twenty five *ddy* strain mice ages ranging from one day, one week, and 1 and 2 weeks, and 2 and10 months. The mice were bred in the laboratory on normal diet and free access to water ad libitum. The animals while under anesthesia were killed by cervical dislocation. The kidney were removed and cut into smaller units and processed following the same procedure as reported earlier (Olea, 1991) as follows; the sections were pre-fixed in a medium containing 2% glutaraldehyde, 0.05M cacodylate buffer (pH 7.2) and 7.5% sucrose for one hour at 4^0C. After fixation, for 30 minutes interval, the specimens were rinsed three times in fresh solution containing sucrose dissolved in 0.05M cacodylate buffer (pH 7.2) at 4^0C and processed for cytochemical study without freezing.

B. Acid Phosphatase Enzyme Cytochemistry

For the elucidation of enzyme activity, the lanthanide–based method for ultrastructural localization of acid phosphatase (AcP) enzyme was employed (Halbhuber *et al*, 1988). Initially, the kidney sections were pretreated with sodium borohydride (0.5mg/ml) in 0.05M tris-maleate buffer (pH7.2) for 60 minutes after the addition 0.1% saponin at room temperature. The tissue sections were then pre-incubated in a medium consisting of the following: 0.05M tris-maleate buffer (pH5.2), 3mM$CeCl_3$ and 10mM 3-amino-1, 2, 4-trizolium for one hour at 37°C in a water bath. Lastly, the tissue sections were incubated in a medium of the same composition containing 15mM β-glycerophosphate for 2 hours at the same condition as the preceding. The specimens were washed overnight in 0.05M cacodylate buffer containing 7.5% sucrose (pH 6.0) at 4°C. For the control, separate tissue sections were incubated in a medium without substrate containing 0.05M cacodylate buffer (pH7.2) and 50mM NaF for one hour at room temperature.

C. Post-Incubation Processing

After washing, the tissue sections were post fixed in a medium containing 1% OsO_4 and 1.5M$K_4Fe(CN)_6$ dissolved in 0.1M cacodylate buffer for one hour at room temperature. The post-fixative medium was freshly prepared before use (Hulstaert *et al*, 1983). The tissue sections were rinsed several times in 0.1M cacodylate buffer dehydrated in a graded series of ethanol and acetone and then embedded in EPON 812 (Tokyo, Japan). Thin sections (0.2µm) were cut using glass knives in a Porter-Blum MT-2B ultra microtome (DuPont Sorvall, U.S.A.) without post staining.

D. Electron Microscopy

1. Qualitative Analysis

X-ray point analysis was done using JEOL JEM4000EX (JEOL, Japan) electron microscope with an attached Tracor Northern, TN-5400 X-ray Analyzer, loaded with routine software. Using TEM, enzyme reaction product present in the lysosome was analyzed for 100s live time at an accelerating voltage of 400kV. The use of high accelerating voltage reported a significant peak-to-background (P/B) ratio (Olea and Nagata, 1991). The size of the beam was set and maintained at 0.5µm. The attached computer has routine software that determines the spectral peak automatically.

2. Quantitative Analysis

For X-ray point quantitative microanalysis, the main spectral line was determined at Lα=4.84 and Lβ=5.26keV and the background was set at Lα=9.400 and Lβ=9.820keV (Olea and Nagata, 1991). The cerium peak reflective of its presence in the lysosome as precipitate and indicative

of the level of AcP activity was determined by the analyzer with routine software attached to the electron microscope.

E. Statistical Analysis

The significance of the results obtained was evaluated using Student's t-test for the difference between means.

RESULTS

A. The Ultrastructural Localization of AcP Enzyme

As shown in Fig. 1, dense reaction precipitate/product was observed over the lysosome, indicative of positive AcP enzyme reaction. Fine ultrastructural localization was observed to be prominent in the proximal tubule cells of the mouse kidney, more specifically on the second segment. However, few or none at all AcP activity was observed in other segments of the mouse kidney. The reaction deposit appeared to be heterogeneous, particularly over the autophagic vacuole (D). However, in some organelles, the reaction deposit due to AcP activity appeared homogeneous (Fig. 2). From the different ages of the animals studied, the reaction deposit was observed to be more intense in one-week-old animals compared to the other age groups. In the control group, where the tissue sections of the animal kidney was incubated with a medium containing no substrate and treated with sodium fluoride (NaF), showed no reaction precipitate over the lysosomes.

B. EM X-ray Point Analysis

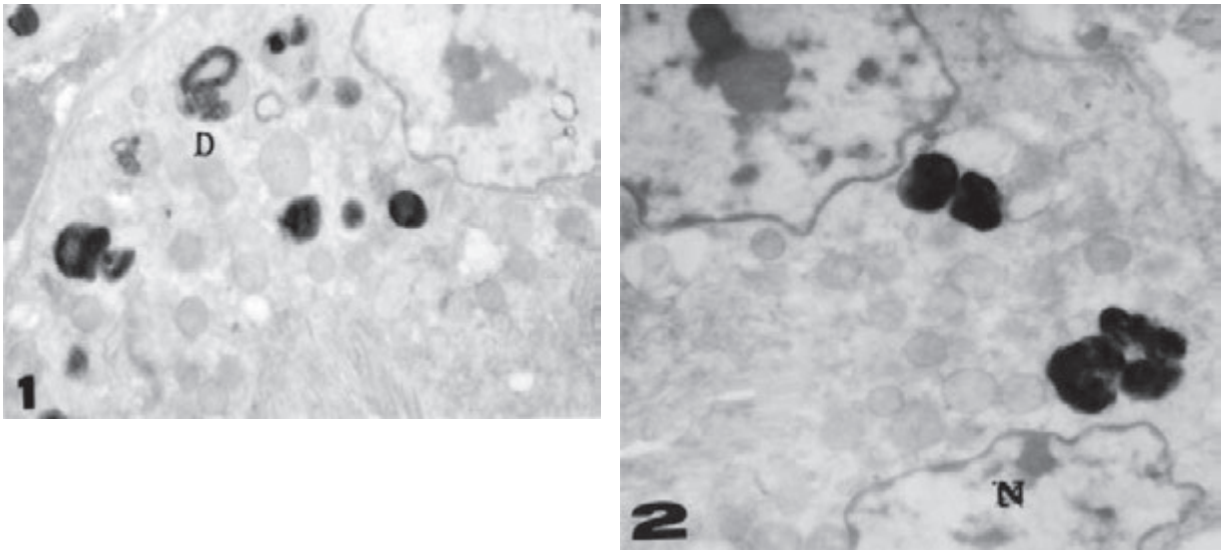

Fig. 1. Electron photomicrograph of a proximal tubule cell of a day old mouse. There are several lysosomes with dense deposit indicative of AcP activity. The dense reaction product appeared heterogeneous, particularly in the autophagic vacuole (D). Unstained (x4800)

Fig. 2. Electron photomicrograph of a proximal tubule cell of one week old mouse. Dense reaction precipitate appeared homogeneous over the lysosomes. (N=nucleus). Unstained (x4800)

1. Qualitative EM Point Analysis

Acid phosphatase (AcP) enzyme localization was demonstrated in the lysosome as a result of the incubation of the tissue sections with a AcP medium containing cerium as the capturing agent. In the dense precipitate, the presence of cerium was determined by x-ray point analysis and reflected in the spectrum. Fig. 4 shows a representative recorded spectrum showing the presence of cerium which was indentified at the range between peak label Lα=4.84keV and Lβ=5.26keV. There were other spectral peaks indentified such as copper (Cu), iron (Fe), osmium (Os) and other

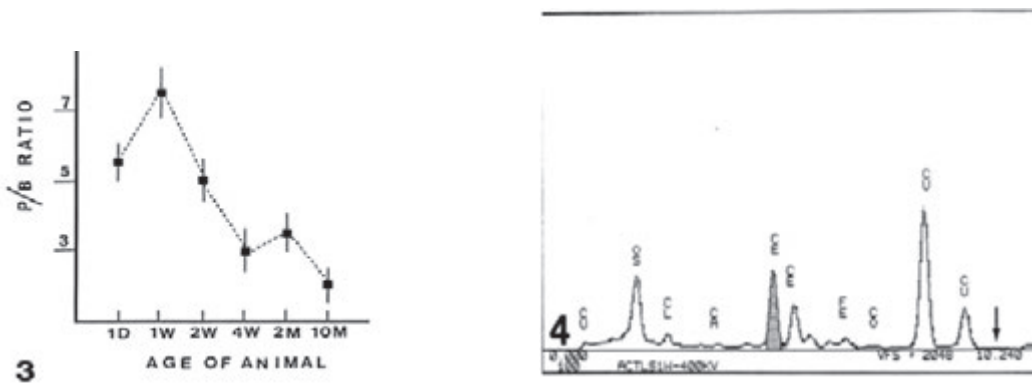

Fig. 3. The transitional curve between acid phosphatase (AcP) enzyme activity in the cellular lysosomes and the different age group of the animal. Mean ±S.D.

Fig. 4. A representative X-ray emission line spectrum from lysosomal precipitate as a result of AcP enzyme activity in one-week-old animal at 400KV. The quantitative analysis (P/B ratio) was determined at Ce (shaded) (Lα=4.84 and Lβ=5.26keV) and the background at (→) (Lα=9.400 and Lβ=9.820keV). Other spectral Peaks: (Ce=cerium, Os=Osmium, Cu=copper, Fe=iron).

minor spectral column.

2. Quantitative EM Point Analysis

The energy dispersive X-ray spectrometer (EDXS) spectrum of cerium in the study of the acid phosphatase (AcP) enzyme activity has been reported earlier (Olea and Nagata, 1991). In the quantitative analysis of enzyme activity using cerium as the capturing agent, spectral peaks were set at peak label Lα=4.84keV and Lβ=5.26keV, respectively. Accordingly, the spectral line of osmium which was determined at label peak Mα=1.914keV has not interfere or influence with the line spectrum of cerium (Van Dort *et al*, 1987). The quantitative analysis of AcP enzyme activity in the lysosome was determined automatically by the attached computer to the electron microscope and the result is reflected as peak-to-background (P/B) ratio. As shown in Fig. 3, the P/B ratio increased from one-day-old, showed a significant increase reaching a peak in one-week-old mice and thereafter, enzyme activity decreased consistently until the 10-month-old animals.

DISCUSSION

There are five important forms of the acid phosphatase (AcP) enzyme found in humans such as prostatic, lysosomal, erythrocytic, macrophagic and osteoclastic (Bull *et al*, 2002). These several enzyme forms were identified to be present in lymphoid organs, liver, spleen, kidney and other tissues (Cerri *et al*, 1999).

Whereas, studies have shown that lysosome contains several enzymes such as acid phosphatase, acid deoxyribonuclease, cathepsin (Yokota and Kato, 1988), arylsulphatase (Goldfischer, 1965) and several other more enzymes, demonstrate that the organelle is indeed involved actively in cellular degradation and/or intracellular digestive processes. However, despite the number of enzymes present in the organelle, only acid phosphatase (AcP) enzyme has been thoroughly studied. Henceforth, acid phosphatase was identified as a marker enzyme for the organelle (Weiss, 1988; Waheed and van Etten, 1985).

When intensive studies have been done on various segments of the mouse kidney, results have shown that lysosomal enzyme activity was more prominent at the proximal tubule, specifically on the second segment (Maunsbach, 1969). The heterogeneity of the reaction observed in some organelles, could be explained by the fact that this segment of the kidney contains varied substrates

like proteins, carbohydrates, sphingolipids and glycoproteins and as such may have been the contributory factor in the heterogeneity of AcP reaction precipitate deposited over the lysosome (Yokota and Kato, 1988; Maunsbach, 1969). Similarly, the same heterogeneity reaction was also observed in other animal tissues and lysosome-like organelles (Bacsy, 1982).

Likewise, the lysosomal enzyme activity is also dependent on the type of animal group, specific stage and site of localization in certain biological processes. For instance, AcP enzyme activity during spermatogenesis was reported to have been localized in the heterophagous lysosome of Sertoli cells in one group of vertebrates studied, while in another group, localization of enzyme activity was observed in the seminiferous epithelium region where the cells are in advanced stage of development (Peruquetti, 2010).

Several studies have shown that the number and volume of lysosome and lysosomal activity is age dependent. In rat liver, it was noted that AcP enzyme activity increased during maturation and declined subsequently during senescence (Schmucker and Wong, 1979). Similar result was observed in the mouse spleen (Olea and Nagata, 1992). In mouse kidney, when the number and size of the lysosome was compared, it was observed that such above-cited variables increase congruently with age of the animal (Olea *et al*, 1991). Likewise, the same study observed that AcP enzyme activity decreased consistently from one day old until the 10-months-old animals. In contrast, the present study determined the AcP enzyme activity in the mouse kidney to have increased initially from a day old, reaching a peak at one-week and then declined consistently until the 10-month-old animals. Somehow, the difference in the quantitative analysis between the previous reports and the present study could be attributed to the electron microscope accelerating voltage (KV) used. Nonetheless, the result of the present undertaking can be substantiated by the fact that at higher accelerating voltage (KV), higher peak and background (P/B) ratio is obtained during the quantification of the enzyme activity in the organelle (Olea and Nagata, 1991).

The result of the AcP enzyme quantitative analysis showed an increase from 1 day old to a week old animals. The increase in the enzyme activity could be attributed to rapid/enhanced process of growth, differentiation and the development of the animal during that stage. As such, it may be construed as a result of accelerated metabolic phagocytosis in the animal cell (Mysliwska *et al*., 1985). As this process continues, a kind of a recycling mechanism may take place in the cellular organelle, and the number of lysosome may no longer change significantly as well as the AcP enzyme activity (Novikoff and Holtzman, 1986). This contention support for the fact that as the animal ages, the AcP enzyme activity decreases as fewer number of kidney cells are expressing positive AcP enzyme (Olea, 1991; Wilson, 1973) and/or showing weak enzyme activity in cells actually showing positive AcP enzyme reaction (Mysliwska *et al*, 1985).

CONCLUSION

Wherefore, from the result of the present undertaking substantiated by the above-cited premise, it could be inferred that acid phosphatase (AcP) enzyme is a marker enzyme for cellular organelle called lysosome. Furthermore, it could be deduced from the results of the present study that cellular lysosomal AcP activity is age-related. Hence, there is an accelerated AcP enzyme activity in the cellular organelles in young mice and that enzyme activity dwindles as the animal ages.

ACKNOWLEDGEMENTS

The present work was a part of a research grant to my father, Prof. Dr. Melanio Trillanes Olea, for foreign researchers from the Japanese Ministry of Education and Culture, Sports, and Science and Technology, under the tutelage of Prof. Dr. Tetsuji Nagata, Professor Emeritus, Shinshu University College of Medicine, Matsumoto, Japan. The critical reading of the manuscript by Prof. Pierre Sebban (University of Paris-Sud11), USTH Rector is highly appreciated.

REFERENCES

Bacsy E (1982) Enzymatic heterogeneity of adrenocortical lysosomes: An X-ray microanalytical study. *Histochem J*. 14:99-112

Blum MS (1970) Invertebrate Testis. In: The Testis. Johanson AD, Gomes WR and Vandemark NL, (eds). Academic Press, London, New York, 393-438

Bowen ID, Lewis GHJ (1980) Acid phosphatase activity and cell death in mouse thymus. *Histochemistry*. 65:173-179

Bull H, Murray PG, Thomas D, Fraser AM (2002) Acid phosphatases. *Mol. Pathol.* 55: 65-72

Cerri LMO, Ajzen S, Arap S, Cerri GG (1999) Ultra-sonografia da Próstata. Sarvier, São Paulo.

Dort van JB, Zeelen, JPH, de Bruijn, WC (1987) An improved procedure for the x-ray microanalysis of acid phosphatase activity in lysosome. *Histochemistry*. 87:71-77

Goldfisher S (1965) The cytochemical demonstration of lysosomal aryl sulfatase activity by light and electron microscopy. *J Histochem Cytochem*. 13:520-522

Hurkadli HK, Hooli MA, Nadkarni VB (1985) Acid phosphate activity in the testis of the Eri silkworm: *Philosamia ricini* (Hutt.) - A histochemical study. *Curr. Sci*. 54: 530-532

Halbhuber KJ, Zimmerman N, Linss, W (1988) New, improved lanthanide methods for the ultrastructural localization of acid and alkaline phosphatase activity. *Histochemistry*. 88:375-381

Hulstaert CE, Kalicharan D, Hardonk MJ (1983) Cytochemical demonstration of phosphatases in the rat liver by cerium-based method in combination with osmium tetroxide and potassium ferrocyanide fixation. *Histochemistry*. 78:71-79

Kuehnel W (2003) Color Atlas of Cytology, Histology, & Microscopic Anatomy (4th Ed.). Thieme. pp. 34

Maunsbach AB (1966) Observations on the segmentation of the proximal tubule in the rat kidney. *J Ultrastruct*. Res. 16:239-258

Maunsbach AB (1969) Functions of lysosome in kidney cells. In: Lysosomes in Biology and Pathology, Vol. 1, Dingle, J. T. and Fell, H. B. (eds), NorthHolland Publ., London, pp.118-154

Mysliwska J, Mysliwska A, Grzegorzewski K, Witkowski J (1985) Age-related changes of activity of acid phosphatase in PHA stimulated lymphocytes. *Exp Geront*. 20:7-14

Novikoff AB, Holtzman E (1986) Cells and Organelles, 2nd ed., Holt, Rinehart and Winston, New York, pp. 135-152.

Olea M T (1991) An ultrastructural localization of lysosomal acid phosphatase activity in aging mouse spleen: A quantitative X-ray microanalytical study. Acta Histochem. *Cytochem*. 24:201-208

Olea M T, Nagata T (1991) X-ray microanalysis of cerium in mouse spleen cells demonstrating acid phosphatase activity using high voltage electron microscope. *Cell. Mol. Biol*. 37(2):155-163

Olea M T, Ma H, Nagata T (1991) Quantitative assessment of lysosomal size, number and enzyme activity in mouse kidney during maturational development. *Cell. Mol. Biol*. 37(7):679-685

Olea M T, Nagata T (1992) Simultaneous localization of 3H-thymidine incorporation and acid phosphatase activity in mouse spleen: Electron microscopic radioautography and cytochemistry. *Cell. Mol. Biol*. 38:115-122

Peruquetti R L, Taboga S R, Azeredo-Oliveira M T V (2010) Expression of acid phosphatase in the seminiferous epithelium of vertebrates. *Genetics and Molecular Research* 9 (2): 620-628 (2010)

Schmucker DL, Wang RK (1979) Rat liver lysosomal enzymes: Effects of animal age and phenobarbitol. *Age*. 2:93-96

Suter A, Everts V, Boyde A, Jones SJ (2001) Overlapping functions of lysosomal acid phosphatase (LAP) and tartrate-resistant acid phosphatase (Acp5) revealed by doubly deficient mice.

Development. 128: 4899-4910

Veenhuis M, Dijken, J P, Harder W (1980) A new method for the cytochemical demonstration of phosphatase activities in yeast based on the use of cerous ions. FEMS Microbiol. Lett. 9; 285-291

Weis L (1988) Cell and Tissue Biology. In: The Cell. Weiss, L (ed.), 6th Ed, Urban and Schwarzenberg, Inc., Germany, pp. 1-66.

Wilson P D (1973) Enzymes changes in ageing mammals. *Gerontologia*. 19:79-125

Yokota S, Kato K (1988) The heterogeneity of rat kidney lysosomes revealed by immuno-electron microscopic staining for cathepsin B and H. *Histochemistry*. 89:499-504

INSTRUCTIONS TO CONTRIBUTORS

Official Journal of the Microscopy Society (Singapore)

Submission of a manuscript implies: (1) that the work described has not been published before (except in the form of an abstract or as part of a published lecture, review, or thesis); (2) that it is not under consideration for publication elsewhere; and (3) that its publication has been approved by all the authors as well as by the responsible authorities at the institute where the work has been carried out. Copyright: when any paper is accepted for publication, the authors agree to automatic transfer of the copyright to the publisher, and that the manuscript will not be published elsewhere in any language without the consent of the copyright holder.

Instructions to contributors

The journal publishes review articles, original research papers, short technical notes, letters to the Editors and short communications on the applications of microscopical techniques and specimen preparation procedures using all forms of microscopes and microanalysers.

Papers must be written in English and should be submitted electronically to the Editor- in-Chief:

Samuel SW Tay
Department of Anatomy, National University of Singapore
Blk MD10, 4 Medical Drive, Singapore 117597
Telephone (65) 6516 3210 Fax (65) 67787643
E-mail: anttaysw@nus.edu.sg

When an article is accepted for publication, the copyright on it passes immediately into the possession of the printer. The copyright covers the exclusive and unlimited rights to reproduce and distribute the article in any form of reproduction (printing, electronic media or any other form); it also covers translation rights for all languages and countries.

No manuscript processing fees, page charges or charges for halftone illustrations will be levied. Authors must prepare manuscripts in accordance with the journal's accepted practice. Authors submitting diskettes are requested to follow the technical instructions printed in each issue of the journal.

Manuscripts should be divided into the following sections: title page; **Abstract; Materials and Methods; Results; Discussion; Acknowledgements; References, figure legends and tables.** The original manuscript must be typed double spaced with wide margins and on one side of the paper only; duplicate copies must be photocopied on both sides of the paper to save on postage. In order to reduce mailing costs, when a manuscript is rejected only the original illustrations will be returned. Genus and species names should be marked with a single straight underline for italics. Words the author wishes to emphasize in the body of the text may also be set in italics and should be marked in the same way. The approximate desired positions of figures and tables should be marked in the margin of the manuscript. For literature citations in the text the name/year system should be used.

Brief accounts of particularly interesting results will be printed out of turn as "Short communications". These should not exceed two or at the most three printed pages.

1. The **title page** must give: first name(s) and surname(s) of author(s); title of the paper; initials(s) of given name(s) and last name(s) of author(s) with full addressees) of institute(s)- any footnotes referring to the title- address to which proofs should be sent and telephone and FAX numbers and e-mail address of the corresponding author.

2. **Abstract**. Each paper should be preceded by a summary not exceeding 200 words.

3. The list of **References** should include only works citied in the text. "Unpublished works" and "personal communications" may be referred to in the text but should not be included in the reference list. References should be listed at the end of the text as follows:
   a) Single author - list alphabetically and then chronologically.
   b) Author and one co-author - list alphabetically by first author and then by co-author and then chronologically.
   c) First author and more than one co-author - list alphabetically by first author and then chronologically, because only the first author's name and "*et al.*" followed by the year of publication will be used in the text.
   d) In the event that more than one paper by the same author or team of authors published in the same year

is cited, the letters a, b, c, etc., should follow the year - e.g., Williamson (1990a) - in both the text and the reference list.

Entries in the reference list should be set out as follows:

Journals: name(s) of author(s) followed by initials (do not use "and")- year of publication; complete title; journal as abbreviated in Index Medicus; volume number, first and last page numbers.

Example:

Andersson H, Bacchi T, Hoechl M, Richtel C (1998) Autofluorescence of living cells. J. Microsc. 119:1-7

Books: name(s) of author(s) followed by initials; year of publication; complete title (in English); edition and volume if appropriate; publisher; place of publication.

Examples:

Books: Klir G.J, Yuan B (1995) Fuzzy sets and fuzzy logic: Theory and application. Prentice Hall Englewood, New Jersey.

Book- chapters: Bach L, Mayer E (1987) Physics of water and ice: implications for cryofixation. In: Steinbrecht RA, Zierold K (eds). Cryotechniques in biological electron microscopy - Springer-Verlag, Berlin, pp 1-34.

4. **Figures**. The illustrations must be submitted in triplicate. Figures should be restricted in number to the minimum needed to clarify the text. Information given in the legends must not be repeated in the text, nor should the same data be presented in both graph and table form. Illustrations that have already been published elsewhere are not usually accepted. All figures, whether photographs, graphs or diagrams, must be numbered in a single continuous sequence in the order in which they are cited in the text. Each figure must be mounted on a separate sheet. The author's name, the number of the figure and the top of the illustration should be indicated on the back or on the sheet it is mounted on.

   Figures can be grouped into a plate with spaces of not more than I mm between the individual illustrations. All figures must he mounted on regular bond paper and not on cardboard. Layouts or single figures should either match the width of a single column (8.6cm) or the printing area (17.6 x 23.6cm). The publisher reserves the right to reduce or enlarge illustrations.
   a) Line drawings: Good-quality prints are needed. The inscriptions must be clearly legible. Letters 2mm high are recommended. Computer drawings are acceptable provided they are of comparable quality to line drawings.
   b) Halftone illustrations: Well-contrasted photographic prints, trimmed at right angles and in the desired final size must be submitted. Inscriptions should be about 3 mm high.
   c) Colour illustrations: There is a page charge if a manuscript contains colour illustrations.

5. **Legends**. Each figure should have a short title followed by a concise description. Magnification of micrographs should be given either in the legend of by a scale bar on the micrograph. Such remarks as: "For explanation, see text" should be avoided. Legends are part of the text and should be appended to it in a list starting on a separate page.

6. **Tables**. All tables must be numbered consecutively with arabic numerals. Each table must be typed on a separate sheet. The title of each table should provide a brief, self-sufficient explanation of its content.

7. **Proofs**. To accelerate publication only one set of proofs will be sent to authors. This will show the final form in which the paper will appear in the journal. Changes made in proof should be limited to the correction of typographical errors. Any others involve time-consuming and expensive work, and the costs will be charged to the author. If necessary, additions may be made at the end of the paper in a "Note added in proof".

8. **Offprints** can be ordered at the time proofs are returned to the publisher.

Microscopy Society (Singapore)

c/o Department of Anatomy, National University of Singapore
4 Medical Drive, MD10, Singapore 117597
http://www.microscopy.org.sg/

Dear Colleagues & Friends,

The **Microscopy Society (Singapore)** is a non-profit think tank actively focused on the promotion of microscopy, organization of microscopy-related activities and facilitation of knowledge and information exchange among its members. With a membership of approximately 100, the society actively promotes and hosts scientific meetings and workshops, and provides scholarships for members to attend conferences.

The society always welcomes new members, and encourages members to actively participate and be involved in organizing microscopy-related activities and events.

Benefits of joining MS(S) include:

- Free subscription to the society's annual scientific journal - ***Annals of Microscopy***
- Free participation in the society's Annual General Meeting, scientific symposia and talks, education workshops, and other events
- Travel scholarships and discounted rates to attend international and regional microscopy-related scientific conferences
- Inclusion in mailing list for special events and forums on microscopy
- Many others

Dr Jeroen Anton van Kan
President

✂----------

MEMBERSHIP APPLICATION FORM

Mr/Ms/Mdm/Dr* _____

Female/Male*

Institution/Company: _____ Position: _____

Address: _____

Tel. No.: _____ (Office/HP) E-mail: _____

Type of Membership: Ordinary/ Corporate*
Membership fees per year: S$ 20.00 (Ordinary Member)
S$ 250.00 (Corporate Member)

Area of Interest: Life Sciences/ Physical Sciences*

Signature: _____ Date: _____
** Please delete where applicable*

Please submit the completed form together with the fees, and for cheque, please make payable to

MICROSCOPY SOCIETY (SINGAPORE) to:

Dr Wu Ya Jun (Hon. Secretary)
c/o Department of Anatomy, Yong Loo Lin School of Medicine, National University of Singapore.
4 Medical Drive,Singapore 117597.

JEOL is a leading global supplier of scientific instruments used for research and development in the fields of nanotechnology, life sciences, optical communication, forensics, biotechnology etc. Utilizing its unique technologies, products, services and knowledge, JEOL helps its customers make significant breakthrough in product development and scientific research. JEOL products include scientific instrumentation and industrial equipment, based on five major product groups:

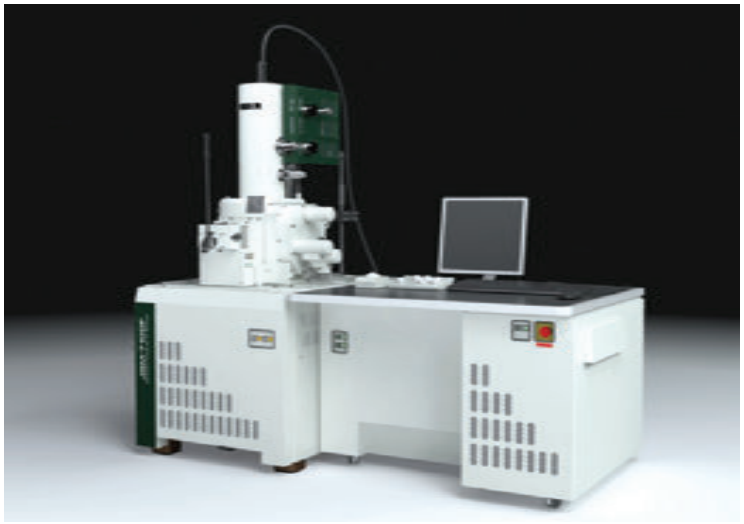

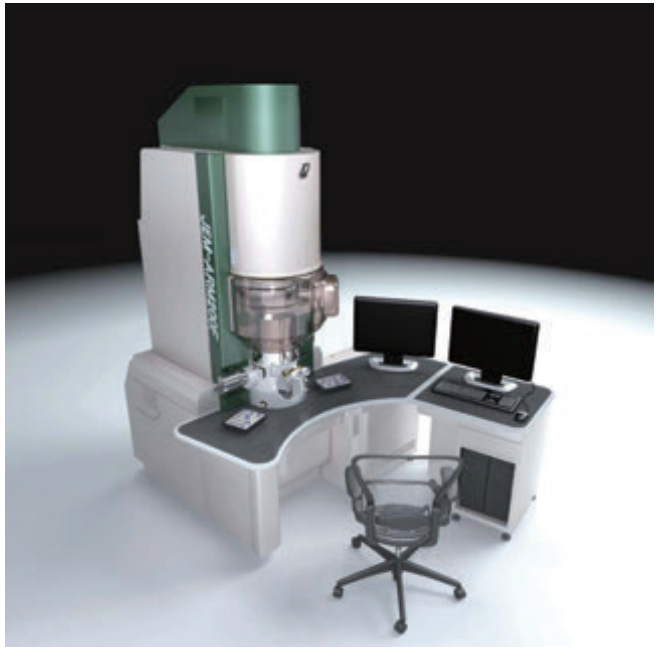

- Electron Optics
- Analytical Instruments
- Semiconductor Equipment
- Thin Film Coating Systems
- Medical Equipment

JEOL Asia Pte Ltd
2 Corporation Road, #01-12
Corporation Place, Singapore 618494
Tel: (65) 65659989, Fax: (65)65657552
e-mail: jeolasia@singnet.com.sg

JEOL
Serving Advanced Technology

HI-TECH INSTRUMENTS

Solutions Beyond Expectation

alicona imaging — The Market Leader in Focus-Variation


3D Surface Metrology


Portable Sensor


Real 3D Rotation


Compact Profiler


Robotic Profiler

EDAX — Results With Confidence


EDS, EBSD & WDS


Micro XRF
(Mono-Capillary Optics)


PC Micro XRF
(Poly-Capillary Optics)

CAMECA — The Reference in Scientific Instrumentation for Micro and Nano-Analysis

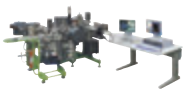
Universal Magnetic
Sector SIMS


Large Radius Magnetic
Sector SIMS


High Resolution
Ion Microprobe


Tomographic Atom Probe


Full Water ULE
Magnetic Sector SIMS


Low Energy X-ray
Emission Spectrometer


Electron Probe Micro-Analyzer

HITACHI — Inspire the Next


In-Lens FESEM


Semi-In-Lens FESEM


Semi-In-Lens FESEM
Super ExB


Semi-In-Lens Schottky
UHR FESEM


Schottky VP-FESEM


Large Chamber VP-SEM


VP-SEM


Compact VP-SEM


Tabletop SEM


FIB


Focused Ion and
Electron Beam


C_s corrected STEM


300kV CFE-TEM


300kV E-TEM


Research BioTEM


3D holder

Revolving holder


3D Tomography image

ION-TOF — Superior Performance for all TOF SIMS Applications

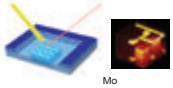
Mo
3D Analysis

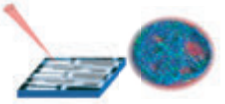
Na, Ser, Lecithin
Surface Imaging

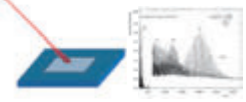
Surface Spectroscopy

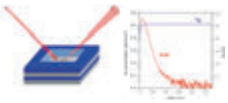
Depth Profiling

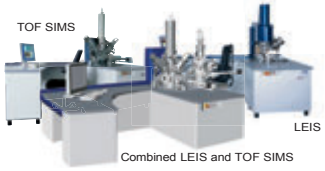

Combined LEIS and TOF SIMS

ksi — We Create SAM-Future


SAM with Scanner Choices
2GHz SAM
Multi-channel SAM

KLA-Tencor — Accelerating Yield


Stylus Profiler
Optical Profiler

Leica MICROSYSTEMS — Living up to Life

SCANCO MEDICAL — The Reference MicroCT - made in Switzerland

Spectral CLSM
Super-continuum Laser
Single Molecule Detection
Super-resolution STED

In Vitro MIcro CT
High Resolution In Vitro MIcro CT
In Vivo (Pre-Clinical)
In Vivo (Clinical)

Preparation to View Information

CPD
Freeze Substiution System
Freeze Drying
Sputter Coater
Glass Knife Maker
Cryo-Microscopy
Ion Miller
Ultramicrotome
High Pressure Freezing

Your Ultimate Strategic Partner

3, Science Park Drive , #04-15 The Franklin, Science Park 1, Singapore 118223 Tel: 65-6899 9218 Fax: 65-6899 0989
Website: http://www.htiweb.com